https://doi.org/10.5194/wes-2026-140
Preprint. Discussion started: 10 September 2026

WIND ENERGY SCIENCE DISCUSSIONS

Mitigating wind farm cluster wakes by vertical staggering

Annika Gaiser[1,2], Gerald Steinfeld[1,2,3], Gabriele Centurelli[1,2], and Martin Kühn[1,2]

[1]Carl von Ossietzky Universität Oldenburg, School of Mathematics and Science, Institute of Physics
[2]ForWind - Center for Wind Energy Research, Küpkersweg 70, 26129 Oldenburg, Germany
[3]Fraunhofer IWES, Küpkersweg 70, 26129 Oldenburg, Germany

Correspondence: Annika Gaiser (annika.gaiser@uol.de)

Abstract. The expansion of offshore wind energy results in more wake influences between wind farms and wind farm clusters, which should be mitigated to reduce negative impacts on the power production. In this study we assess whether vertical staggering of wind turbine heights within a wind farm could mitigate farm wake interaction between two neighbouring wind farms. The aim is to understand how wake recovery mechanisms and three-dimensional wake characteristics differ between vertically staggered and non-staggered wind farms. We performed large-eddy simulations of a pair of an upstream and a downstream wind farm in a conventionally neutral atmospheric boundary layer and compared several vertical staggering layouts at the upstream wind farm to the non-staggered reference. To assess differences, we analysed mean wake characteristics, the three-dimensional flow field, the wake recovery budget, and power production. We found that vertical staggering hindered the mean wake recovery of the horizontal wind speed at the hub height of the lower turbines by reducing momentum at higher altitudes. Investigating spatial wind fields revealed a more heterogeneous, narrower farm wake with streaks of increased wind speeds for vertically staggered wind farms. The wake differences were explained by the formation of larger-scale advective flow structures for vertically staggering cases and their larger contribution to the mean wake recovery compared to turbulent mixing. A circulation zone at the northern wake edge was present for staggered and non-staggered setups, which caused a streak of increased wind speeds in the lower half of the boundary layer. The wake heterogeneities persisted far downstream and impacted the wake and power production of the non-staggered, downstream wind farm, causing locally increased or decreased power. The total power production of the vertically staggered upstream wind farm was strongly increased due to higher wind speeds at the taller turbines, a lower rotor density per height, and a better wake recovery at lower hub heights inside the wind farm. To conclude, we showed that vertical staggering has the potential of locally improving the farm wake recovery by creating or enhancing large-scale advective flow structures, influencing the wake and power of a downstream wind farm. The advection-driven recovery of the far farm wake is relevant for wind farms beyond vertically staggered setups, requiring future analyses to focus on production mechanisms of large-scale advective structures.

1 Introduction

Wind farms in a marine environment produce wake regions that can reach extents of multiple tens of kilometres, as has been shown with airborne, lidar, and satellite aperture radar (SAR) measurements (Platis et al., 2018; Schneemann et al., 2020). With the expansion of offshore wind energy, it is common that new wind farms are installed within these distances to other

https://doi.org/10.5194/wes-2026-140
Preprint. Discussion started: 10 September 2026

eawe european academy of wind energy
Open Access WIND ENERGY SCIENCE DISCUSSIONS

wind farms inside the same or a different wind farm cluster. Therefore, the wakes of large wind farms or agglomeration of wind farms, in the following referred to as cluster wakes, can negatively impact the power production of neighbouring wind farms (Schneemann et al., 2020; Borgers et al., 2025). Investigating potential methods to tailor the flow inside and around wind farms to mitigate the extent and intensity of cluster wakes has thus gained increasing importance during the past years.

To understand how cluster wakes can be mitigated we first need to understand which mechanisms drive the cluster wake recovery. Contrary to the recovery of a single turbine or small wind farms, next to the vertical turbulent transport also transport by the mean flow is relevant (Kasper and Stevens, 2026). The relevant mechanisms differ along the downstream distance of the wind farm. In the first few kilometres downstream of the wind farm, the recovery is mainly driven by turbulence (Syed et al., 2023; Lanzilao and Meyers, 2025). Turbine wakes are modified by an increased divergence of the vertical turbulent momentum flux, which causes vertical entrainment of higher momentum from above the wind farm and results in a comparably fast wake recovery. Further downstream, the net vertical turbulent momentum flux approaches the negative inflow value, thus not recovering the wind speed in the far wake (Lanzilao and Meyers, 2025; Maas and Raasch, 2022). Instead of turbulent mixing, advective processes become relevant for the wake recovery in the far cluster wake. Lanzilao and Meyers (2025) describe in large-eddy simulations (LES) a lateral entrainment that mainly occurs at the right wake edge on the northern hemisphere and adds momentum from the side, slowly recovering the wake over long distances. Another fundamental mechanism in the recovery of the far cluster wake is the pressure gradient driving the geostrophic wind. For large wind farms, the counterclockwise wake deflection on the northern hemisphere and the boundary layer growth can increase the wake recovery through the geostrophic pressure gradient (Maas and Raasch, 2022).

The magnitude of the recovery depends on the atmospheric conditions, resulting in differing cluster wake characteristics for different atmospheric boundary layers (ABL). One major influencing factor for the wake extent is the atmospheric stability. In particular, stable boundary layers promote longer wake extents than neutral or convective boundary layers, due to lower turbulence (Platis et al., 2018). Furthermore, the ABL height can influence the wake width and the formation of more complicated advective flow structures (Lanzilao and Meyers, 2025). For instance, in shallow conventionally neutral boundary layers (CNBLs), wind farms can create circulation zones that influence the wake development (Lanzilao and Meyers, 2025). On larger scales, wind farm wakes can be deflected. A clockwise deflection on the northern hemisphere is caused by veer together with vertical turbulent transport and negative perturbation pressure (Laan and Sørensen, 2017; Maas and Raasch, 2022; Ouro et al., 2025). For larger wind farms, Maas and Raasch (2022) found in the Weather Research and Forecasting model (WRF) a counterclockwise deflection, because of an increasing role of the decreasing Coriolis force related to smaller wind speeds. The strong dependence of cluster wake characteristics on atmospheric conditions emphasises the need to model realistic atmospheric conditions such as CNBLs that include the influence of veer and a capping inversion.

Since the wakes of large wind farms can reach multiple tens of kilometres downstream, the power production and wakes of neighbouring wind farms can be influenced. Many studies describe a wind speed and power reduction at a wind farm located in

https://doi.org/10.5194/wes-2026-140
Preprint. Discussion started: 10 September 2026

eawe european academy of wind energy
Open Access WIND ENERGY SCIENCE DISCUSSIONS

the wake of an upstream wind farm. According to the LES study by Stieren and Stevens (2022), this power reduction is present throughout the entire downstream wind farm. The distribution of the power production within the downstream wind farm can be heterogeneous if the waked inflow is characterised by regions of lower and higher wind speeds (Nygaard and Hansen, 2016; Schneemann et al., 2020), which can for instance be caused by speed-up regions at the wake boundary (Nygaard and Hansen, 2016). Stieren and Stevens (2022) compared in LES the wake recovery between an upstream and a downstream wind farm in a completely neutral boundary layer (NBL). They described that remnants of the upstream cluster wake can still result in increased turbulence intensity behind the downstream wind farm, resulting in a faster wake recovery. As described previously, this might be specific to the simulated atmospheric conditions, since other studies on CNBLs found a less far-reaching impact of turbulence in the wake (Lanzilao and Meyers, 2025). Compared to an upstream wind farm, flow deflection over the downstream wind farm and related boundary layer growth is smaller, since a negative vertical velocity in the wake of the upstream wind farm hinders the deflection at the beginning of the downstream wind farm (Stieren and Stevens, 2022).

Considering the mostly negative impacts on a downstream wind farm, multiple studies have investigated how different static or dynamic factors influence the wake characteristics and partly looked into mitigation strategies. One idea behind cluster wake mitigation is to challenge the current approach of a greedy wind farm that tries to maximise its own power without considering effects on downstream wind farms. Collaborating on wind farm cluster optimisation rather than individual wind farm optimisation could provide beneficial outputs (Foloppe et al., 2023). Since wake recovery is driven by turbulence, one approach could be the enhancement of turbulence, e.g. by implementing active cluster wake mixing strategies. Gutknecht et al. (2024) implemented in LES an active cluster wake mixing strategy, which excites the turbine thrust in a pattern that propagates through the wind farm. This approach could influence the cluster wake by changing turbulence, but the impact on the downstream power production was minor. The turbine thrust can also be used in a passive way to affect the wake by using turbine concepts with different properties. Paulsen et al. (2026) implemented in WRF a new turbine concept with low specific rating and low induction on all existing and planned wind farms in the German Bight and found positive impacts on the overall power production. The influence on the wake varied depending on the wind speed, causing stronger wake deficits for low wind speeds due to a larger power production and smaller wake deficits for high wind speeds due to lower thrust coefficients of the new turbine concept. Another goal could be the reduction of inner-farm wake overlap, which could decrease the total wake intensity. Reducing inner-farm wake effects can among others be achieved by tilting the rotor. Kasper and Stevens (2024) investigated in LES positive and negative rotor tilt, which increased the power production of an upstream wind farm with an aligned setup and might benefit at least the first rows of a downstream wind farm. Another approach for reducing wake overlap could be the implementation of different turbine heights within a wind farm cluster. Syed et al. (2020) analysed with WRF repowering strategies that use varying hub heights with the aim of mitigating wind farm wakes inside a wind farm cluster. They found that placing turbines to higher hub heights can reduce wake overlap and thus increase power production. The approach of placing turbines with different hub heights within a wind farm is referred to as vertical staggering.

https://doi.org/10.5194/wes-2026-140
Preprint. Discussion started: 10 September 2026

WIND ENERGY SCIENCE DISCUSSIONS
Open Access
eawe european academy of wind energy

Previous studies investigated whether vertically staggered wind farms could be used to increase the power production of a single wind farm and how the inner-farm wakes are affected. In LES studies, vertically staggered wind farms were manually created by either adding smaller turbines to a wind farm (Chatterjee and Peet, 2019) or diverging the hub heights of the existing turbines to lower and higher altitudes (Lu et al., 2025; Wang et al., 2025; Wu et al., 2018; Zhang et al., 2018). Other studies applied optimisation models to develop wind farm layouts with the highest possible AEP, optimising for the hub height (Sun and Yang, 2023; Vasel-Be-Hagh and Archer, 2017) and in Sun and Yang (2023) additionally for the wind farm layout. All of these studies found that a vertically staggered wind farm can increase the power production, although Zhang et al. (2018) also described a setup with strongly overlapping wake areas that resulted in a smaller power output. This is supported by the findings of Lu et al. (2025); Vasel-Be-Hagh and Archer (2017); Wang et al. (2025) that larger hub height differences give rise to larger increases in power production of the staggered windfarm. The main reason for the power increase was a less disturbed inflow for turbines in the first few rows (Zhang et al., 2018). Depending on the vertical wind profile and turbine hub height, taller turbines can receive higher wind speeds, resulting in more power and a stronger wake deficit compared to lower altitudes (Wu et al., 2018). Additionally, changes in the turbulence or flow advection are relevant. Downdrafts of kinetic energy by large-scale flow structures could increase the efficiency of additional smaller turbines. On the contrary, for a different setup with added turbines at an intermediate height the mixing of wakes suppressed such downdrafts and resulted in a lower efficiency for these additional turbines (Chatterjee and Peet, 2019). For a vertically staggered wind farm with alternating rows of high and low turbines, higher vertical kinetic energy fluxes can be present due to higher turbulence mixing in the shear layer compared to a non-staggered wind farm, as shown by a wind tunnel study by Chamorro et al. (2014). This was however not confirmed by Zhang et al. (2018), who found in LES no increase in the vertical kinetic energy flux. Furthermore, Zhang et al. (2018) found that in the presence of taller turbines lower turbines are rather shielded from the undisturbed flow, hindering the recovery of their wakes inside the wind farm. The cluster wake was so far barely analysed, only Wang et al. (2025) described a shorter wake for vertically staggered wind farms. Since some studies described a higher vertical kinetic energy flux or downdrafts related to large-scale flow structures, this could result in an improved recovery of the cluster wake of a vertically staggered wind farm.

Overall, studies that analyse the influence of different factors on the wake characteristics and recovery mechanisms of large wind farms are still rare. Few studies looked into possible mitigation strategies and showed promising starting points on influencing the cluster wake. One possible influencing factor that has not been investigated yet for cluster wakes is vertical staggering. Studies on vertically staggered wind farms mainly focused on quantification of the inner-farm wake characteristics and power production rather than exploring the underlaying flow physics. When wake recovery mechanisms inside the wind farm were analysed, the focus was usually put on the turbulent vertical momentum flux, mostly neglecting other potential influences of the wake recovery budget that could be affected by vertical heterogeneity of the wind farm. Detailed analyses on the wake recovery mechanisms and three-dimensional flow field inside and downstream of vertically staggered wind farms are still missing. Since previous studies indicated a possible influence of vertical staggering on turbulence as well as large-scale flow structures, vertically staggered wind farms might influence advective wake recovery mechanisms and therefore the far wake recovery. The analysis of the far wake recovery becomes especially relevant for CNBLs. So far, most studies focused on

https://doi.org/10.5194/wes-2026-140
Preprint. Discussion started: 10 September 2026

eawe european academy of wind energy
Open Access WIND ENERGY SCIENCE DISCUSSIONS

neutral boundary layers without a capping inversion, excluding the effects of a veered boundary layer and Coriolis effects that showed to be relevant for the far wake recovery in previous studies on large offshore wind farms.

To close these knowledge gaps, our objectives are twofold: first, understanding how the turbulent and advective flow recovery mechanisms in a conventionally neutral boundary layer are affected by vertically staggered wind farms and second, investigating how wind flow can be tailored inside and downstream of large wind farms in pursuit of cluster wake mitigation. In particular, we address three aspects to improve our insight in the flow physics of cluster wakes. First, we identify how vertically staggered wind farms affect cluster wake characteristics compared to a non-staggered wind farm. We investigate these wake differences by comparing wake recovery budgets and characteristics of the three-dimensional flow field. Second, we examine how the wake of a vertically staggered wind farm influences the inner farm and cluster wake of a downstream wind farm. Third, we assess how vertically staggered wind farms affect their power production and the power production of a downstream wind farm.

2 Methods

In the methods section, we first describe the functioning of the simulation model and the model setup (Sect. 2.1), as well as the wind farm setup (Sect. 2.2). Then, the atmospheric boundary layer conditions are described (Sect. 2.3), and finally the analysis approach (Sect. 2.4).

2.1 Model setup

We performed our research with LES, using the Parallelised Large-eddy Simulation Model (PALM) version 23.10 (Maronga et al., 2020). PALM is an incompressible code, resulting in a divergence-free LES-filtered flow field. The governing equations of the flow are (Maronga et al., 2020):

$$\frac{\partial \widetilde{u}_j}{\partial x_j} = 0, \tag{1}$$

$$\frac{\partial \widetilde{u}_i}{\partial t} = -\frac{\partial \widetilde{u}_i \widetilde{u}_j}{\partial x_j} - \varepsilon_{ijk} f_j \widetilde{u}_k + \varepsilon_{i3j} f_3 u_{g,j} - \frac{1}{\rho}\frac{\partial \pi^*}{\partial x_i} + g\frac{\widetilde{\theta}_v - \langle \theta_v \rangle}{\langle \theta_v \rangle}\delta_{i3} - \frac{\partial}{\partial x_j}\left(\widetilde{u_i'' u_j''} - \frac{2}{3} e_{\mathrm{SGS}} \delta_{ij}\right) + d_i \tag{2}$$

$$\frac{\partial \widetilde{\theta}}{\partial t} = -\frac{\partial \widetilde{u}_j \widetilde{\theta}}{\partial x_j} - \frac{\partial}{\partial x_j}\left(\widetilde{u_j'' \theta''}\right) \tag{3}$$

The streamwise, crosswise, and vertical direction (x, y, z) or component (e.g. velocity u, v, w) are defined with $i, j, k \in (1, 2, 3)$. Depending on i, j, k the Levi-Civita symbol ε_{ijk} and Kronecker delta δ_{ij} are calculated. LES filtering is indicated with a $\sim$. The Coriolis parameter f_j is determined from the Earth's angular velocity Ω, latitude Φ, and rotation angle of the domain α: $f_i = (-2\Omega\cos(\Phi)\sin(\alpha), 2\Omega\cos(\Phi)\cos(\alpha), 2\Omega\sin(\Phi))$. The geostrophic wind speed components are $u_{g,j}$, the virtual potential temperature is θ_v, and the gravitational acceleration is g. The subgrid-scale turbulent kinetic energy (SGS-TKE) is defined as $e_{\mathrm{SGS}} = \frac{1}{2}\widetilde{u_i'' u_i''}$. The modified perturbation pressure is defined as $\pi^* = p^* + \frac{2}{3}\rho e_{\mathrm{SGS}}$ with the perturbation pressure p^* and

https://doi.org/10.5194/wes-2026-140
Preprint. Discussion started: 10 September 2026

air density ρ. The forces of the wind turbines are represented by d_i.

The wind turbines were modelled with an actuator disk model with rotation (ADM-R) similar to the one described by Wu et al. (2011). The ADM-R is based on the blade element momentum theory and considers in addition to the thrust also the torque. A detailed description is given in Maronga et al. (2020). The yaw angle of the turbines was set to adapt to the prevailing wind direction.

The simulations were performed by a sequence of precursor and main runs. The precursor had a domain extent of $5.76\ \mathrm{km} \times 5.76\ \mathrm{km} \times 21.15\ \mathrm{km}$ with a grid spacing of $20\ \mathrm{m} \times 20\ \mathrm{m} \times 10\ \mathrm{m}$ and was run for $50\ \mathrm{h}$, a time sufficient to reach a quasi-steady state where the domain-averaged total kinetic energy and vertical velocity profiles do no longer significantly change in time. The prognostic variables of the precursor were used to initialise the main run by deriving the mean inflow conditions from the averaged profiles which were present at the end of the precursor and including the turbulence statistics. Two main run setups were created, depending on whether one or two wind farms were included (Sect. 2.2). The main runs with one wind farm had a domain extent of $115.20\ \mathrm{km} \times 40.96\ \mathrm{km} \times 21.15\ \mathrm{km}$ and the runs with two wind farms $153.60\ \mathrm{km} \times 40.96\ \mathrm{km} \times 21.15\ \mathrm{km}$ (Fig. 1). The grid spacing was $20\ \mathrm{m} \times 20\ \mathrm{m} \times 10\ \mathrm{m}$ to have at least twelve grid cells along the rotor diameter (Sect. 2.2). The extent in y was selected to be six times as large as the wind farm width to avoid blockage effects of the domain boundaries. In z-direction, the grid was stretched from $1.5\ \mathrm{km}$ upwards with a stretching factor of 1.06 and a maximum grid spacing of $50\ \mathrm{m}$. Above $3.6\ \mathrm{km}$ Rayleigh damping was applied to dampen gravity waves. This Rayleigh damping height was selected to include at least two gravity-wave wave lengths above the capping inversion. A recycling domain spanned from the domain start to $5.8\ \mathrm{km}$ downstream of the domain start and was used to maintain the turbulent inflow. The boundary conditions of the main run included at the west boundary an inflow. For all prognostic variables, except for the potential temperature, a Dirichlet boundary condition is set and turbulent fluctuations are recycled from the recycling plane. For the potential temperature absolute values are recycled to avoid thermal instabilities at the inflow plane (Centurelli et al., 2025). For the perturbation pressure a Neumann boundary condition is set. The east boundary had an outflow radiation boundary condition. The north and south boundary had periodic boundary conditions. Further specifications of the boundary conditions can be found in the namelist file, which is available in the link found in the data availability statement. The domains were located on the northern hemisphere at a latitude of 54° N. The roughness length was 0.002 m. The simulations were run for $4.4\ \mathrm{h}$ for the shorter domain and $5.5\ \mathrm{h}$ for the longer domain. This included the spin-up time, which was the time the flow at baseline hub height needs to travel to the entire domain once, and $1\ \mathrm{h}$ of data collected for the analysis. This simulation time was sufficient to calculate meaningful statistics.

2.2 Wind farm setup

The baseline setup (B1) was inspired by Stieren and Stevens (2022) and consisted of two wind farms with 72 IEA 15 MW turbines, respectively (Fig. 1). The IEA 15 MW turbine has a hub height (z_{hub}) of 150 m and a rotor diameter (D) of 240 m (Gaertner et al., 2020). The turbines were set in an aligned setup with a spacing between the wind turbines of $s_x = 7D$ in streamwise direction and $s_y = 5D$ in crosswise direction. The distance of the upstream wind farm to the inflow plane was

https://doi.org/10.5194/wes-2026-140
Preprint. Discussion started: 10 September 2026

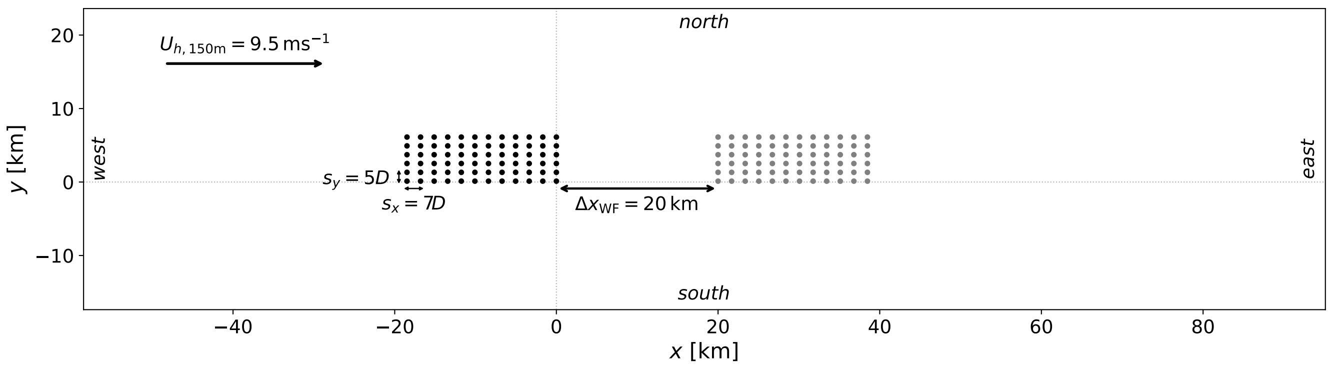

Figure 1. Main domain including two wind farms, the upstream wind farm (WF1) in black and the downstream wind farm (WF2) in grey. Each dot represents one wind turbine. The westerly inflow wind direction is indicated by the black arrow. The origin of the coordinate system is in streamwise direction at the end of WF1 and in crosswise direction at the southern wind farm edge.

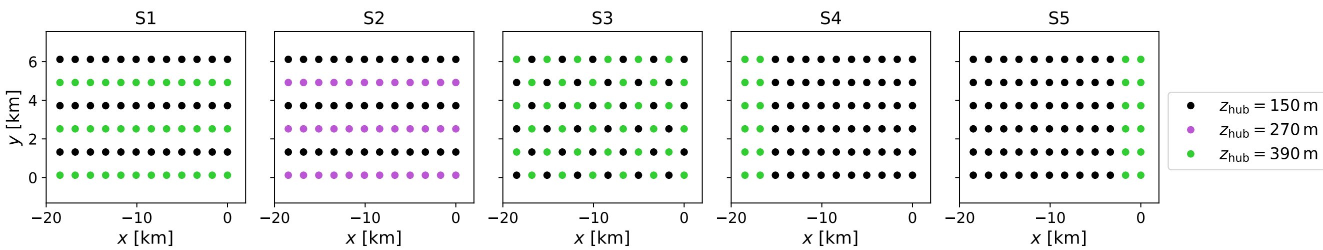

Figure 2. Vertical staggering setups S1-S5. The colouring shows which turbines have a larger hub height compared to the baseline setup. The results of S4 and S5 are only addressed in the appendix.

40 km so that the blockage effect does not reach the recycling plane. The distance between the two wind farms was chosen as 20 km ($\approx 83D$), which is the distance after which the farm wake recovered similar for all setups (Sect. 3.1.1). The two wind farms were situated in the centre of the model domain with respect to the y-direction. This setup was simulated twice, once only including the upstream wind farm (WF1) and once including additionally the downstream wind farm (WF2). All five vertical staggering setups were done once including only WF1 and two selected setups were repeated including WF2 (Tab. 1). This was done to be able to first analyse the impact of vertical staggering on the cluster wake and afterwards analyse its effect on the downstream wind farm. For the comparison of the power production an additional baseline setup (B2) with one uniform hub height at the highest staggering hub height of 390 m was performed.

To create a vertically staggered wind farm, the hub height of a portion of the simulated wind turbines was changed. Previous studies either added smaller turbines or changed the hub height of existing turbines to lower and higher altitudes. In our study we maintained the total number of turbines and wind farm power. Contrary to the other studies, we kept some turbines at their baseline hub height and only increased the hub height of selected turbines. Thereby we can assess how the wake and power

Table 1. Summary of the baseline (B) and vertical staggering (S) setups. The column "Wind farms" shows whether the setup was run only for the upstream wind farm (WF1) or for the upstream and downstream wind farm (WF1+WF2). WF2 was in all cases a non-staggered setup with all turbines at 150 m hub height.

Setup	Description of WF1	Wind farms
B1	Baseline setup 150 m hub height	WF1, WF1+WF2
B2	Baseline setup 390 m hub height	WF1+WF2
S1	Alternating columns of low and high wind turbines without overlapping rotor area.	WF1, WF1+WF2
S2	Alternating columns of low and high wind turbines with overlapping rotor area.	WF1
S3	Every second wind turbine higher, along the x- and y-direction respectively.	WF1, WF1+WF2
S4	First two rows with high wind turbines. (Appendix A1)	WF1
S5	Last two rows with high wind turbines. (Appendix A1)	WF1

output of the baseline turbines change without facing a change in wind conditions that would occur if we changed all turbines to higher and lower altitudes. To avoid further influencing factors, we kept other turbine properties like the rotor diameter and the blade characteristics unchanged. From an engineering point of view this would be hard to realise concerning the loads, but was justified for our study, since we wanted to provide a physical proof of concept and did not aim to analyse potentially realistic setups. Since previous studies found most pronounced differences for larger hub height differences, when the wakes of different heights interact as little as possible, we set the hub heights of the taller turbines either to 270 m or to 390 m, i.e. to have half of the rotor area overlapping or no overlap in rotor area, respectively. By having vertical staggering setups without overlapping rotor areas, potential vertical staggering effects on the flow should appear more clearly, allowing a more thorough analysis of the physical processes. The setups with overlapping rotor areas allowed to test the sensitivity to the hub height difference. In total, five setups were created, which are summarised in Table 1 and visualised in Fig. 2. Two of these setups, S4 and S5, were excluded from the main results and added to the appendix (A1).

2.3 Atmospheric boundary layer conditions

The flow was characterised by a CNBL with an atmospheric boundary layer (ABL) height of 570 m (Fig. 3). The ABL height was here defined as the height with the strongest temperature gradient (Sullivan et al., 1998). The lapse rate of the capping inversion (CI) was 0.04 $\mathrm{K\,m^{-1}}$ and of the free atmosphere 0.01 $\mathrm{K\,m^{-1}}$ (Fig. 3(c)). The mean wind speed at the IEA 15 MW hub height of 150 m was 9.5 $\mathrm{m\,s^{-1}}$ and the turbulence intensity (TI) was 4.4 %. For the increased hub height in the vertical staggering setups, the horizontal wind speed reached up to 10.4 $\mathrm{m\,s^{-1}}$ at 390 m (Fig. 3(a)), which was just below the rated capacity, and the turbulence intensity decreased to 2.6 %. The wind veer was around 3° over the baseline IEA 15 MW rotor extent and 7° over the entire vertical staggering height extent (Fig. 3(b)). All implemented wind turbines were fully inside the ABL and the highest wind turbines reached with their rotor tip up to 510 m, so around 60 m less than the converged ABL height.

https://doi.org/10.5194/wes-2026-140
Preprint. Discussion started: 10 September 2026

eawe european academy of wind energy
Open Access WIND ENERGY SCIENCE DISCUSSIONS

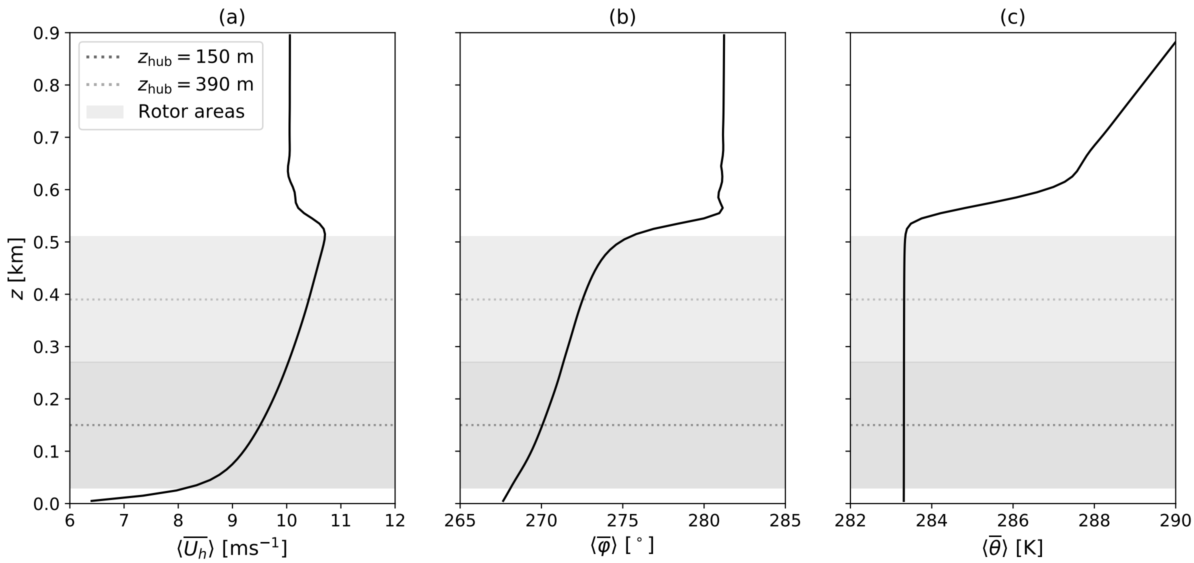

Figure 3. Vertical profile of the temporally and spatially averaged (a) horizontal wind speed $\langle\overline{U}_h\rangle$, (b) wind direction $\langle\overline{\varphi}\rangle$ and (c) potential temperature $\langle\overline{\theta}\rangle$ in the undisturbed inflow.

2.4 Analysis approach

All analyses were performed on temporally averaged variables, which is marked by an overbar $(\bar{\cdot})$. A spatial average is indicated by angular brackets $\langle\rangle$. The horizontal wind speed was calculated as $U_h = \sqrt{u^2+v^2}$, the TKE as $e = 0.5\left(\overline{u'^2}+\overline{v'^2}+\overline{w'^2}\right) + e_{\mathrm{SGS}}$ and the turbulence intensity as $\mathrm{TI} = \sqrt{\frac{2}{3}e}/U$, where u', v', w' were the turbulent fluctuations around the mean part $\overline{u}, \overline{v}, \overline{w}$ as defined by the Reynolds decomposition $u_i = \overline{u_i} + u_i'$.

Values of the undisturbed inflow are marked by ∞ and usually its value at the respective height was used for a normalisation, e.g. the normalised horizontal wind speed was $U_h/U_{h,\infty}$. In the following, the term “inflow” refers to the undisturbed inflow that was not affected by the global blockage of the wind farm.

For the figures, scientific colour maps by Crameri et al. (2020) were used.

The wake recovery budget is calculated similar to Boudreau and Dumas (2017) and is based on the governing equation Eq. (2), where the left side equals to zero due to stationary conditions. The equation was solved for the temporally averaged and LES-filtered streamwise velocity component u, and normalised with the streamwise wind speed component $\overline{u}$, resulting in the change of velocity in space [s^{-1}]:

$$0 = \overbrace{-\frac{\partial \bar{u}}{\partial x}}^{\mathcal{R}} \overbrace{-\bar{v}\frac{\partial \bar{u}}{\partial y}\frac{1}{\bar{u}}}^{\mathcal{A}_y} \overbrace{-\bar{w}\frac{\partial \bar{u}}{\partial z}\frac{1}{\bar{u}}}^{\mathcal{A}_z} \overbrace{+(f_3\bar{v} - f_2\bar{w})\frac{1}{\bar{u}}}^{\mathcal{C}} \overbrace{-f_3\overline{v_g}\frac{1}{\bar{u}}}^{\mathcal{P}_g} \overbrace{-\frac{1}{\rho}\frac{\partial \pi^*}{\partial x}\frac{1}{\bar{u}}}^{\mathcal{P}^*} \overbrace{-\frac{\partial}{\partial x_j}\left(\overline{u'u_j'} - \overline{\tau_{1j}}\right)\frac{1}{\bar{u}}}^{\mathcal{T}_j} \quad (4)$$

https://doi.org/10.5194/wes-2026-140
Preprint. Discussion started: 10 September 2026

The first term on the right side of the equation, the streamwise recovery term $\mathcal{R}$, quantifies whether the wind speed recovers in streamwise direction. The streamwise recovery term is based on the streamwise advection term $-\overline{u}\partial_x\overline{u}$, divided by the streamwise wind speed component $\overline{u}$. A negative recovery term $\mathcal{R}$ indicates a recovery of the wind speed deficit and a positive recovery term indicates a strengthening of the deficit in streamwise direction. In stationary conditions, the streamwise recovery term $\mathcal{R}$ is balanced by the remaining terms of Eq. 4, which determine the magnitude and sign of the recovery term. These terms are: the crosswise and vertical advection $\mathcal{A}_y$ and $\mathcal{A}_z$; the divergence of the turbulent momentum fluxes in streamwise, crosswise and vertical direction combined with the SGS shear stresses $\mathcal{T}_x$, $\mathcal{T}_y$, and $\mathcal{T}_z$; the perturbation pressure gradient $\mathcal{P}^*$; the Coriolis term $\mathcal{C}$; and the geostrophic pressure gradient balancing the Coriolis force in the free atmosphere, in the following referred to as pressure term $\mathcal{P}_g$. Except for $\mathcal{R}$, all terms that are positive contribute to wake recovery and negative terms hinder the wake recovery.

To analyse the changes in the mean budget terms in streamwise direction, we averaged the budget over the wind farm width. Since gravity waves were present (Lanzilao and Meyers, 2025), we applied a low-pass filter along the streamwise direction over the length of two gravity waves (≈ 6.6 km) to remove related oscillations and be able to better analyse the mean budget components. By averaging over the wind farm width we might have some inaccuracies in the included wake area, since the wake boundary is not equivalent to the wind farm boundary, but this way we kept the averaging area constant and, at the location of a potential second wind farm, still included the entire wind farm extent. To identify changes in the budget terms over the wind farm width, we plotted the budget also over the crosswise direction at different downstream distances, for which we applied a moving average to remove smaller fluctuations.

The wake width was defined as the distance between the left and right wake edge at each x-location behind the wind farm. The wake edge was defined as 97 % of the temporally averaged horizontal inflow wind speed. We implemented this definition based on previous studies defining the internal boundary layer height, so the upper wake boundary, as 97 % of the horizontal inflow wind speed (Maas and Raasch, 2022).

3 Results

The following three sections describe the impacts of vertically staggered wind farms on the flow and power production. First, we analyse the wake of a single wind farm with different setups (Sect. 3.1) to gain an understanding on how vertical staggering influences the external wake characteristics. Second, we investigate how these wakes of an upstream wind farm with varying setups impact the wake of a downstream wind farm (Sect. 3.2). Third, we compare the power production of both wind farms between the setups and relate them to the described wake differences (Sect. 3.3).

https://doi.org/10.5194/wes-2026-140
Preprint. Discussion started: 10 September 2026

3.1 Wake characteristics of a single vertically staggered wind farm

When comparing the wake of vertically staggered wind farms to non-staggered wind farms a one-dimensional analysis at a single hub height is not sufficient. The vertical extent and three-dimensional wake structure also need consideration. First, we focus on the mean wake characteristics at baseline hub height and averaged over the entire wind farm height, as well as vertical profiles at two distances behind the wind farm (Sect. 3.1.1). Second, we explain described differences with the wake recovery budget (Sect. 3.1.2). To gain further understanding of the underlying physical processes, we analyse for selected vertical staggering setups the three-dimensional flow field and characterise two relevant flow patterns in more detail (Sect. 3.1.3).

3.1.1 Mean wake extent and intensity of different vertically staggered wind farm setups

First, we compare the mean flow inside the wind farms at the baseline hub height of 150 m (Fig. 4(a)). All of the here described vertical staggering setups result in a wind speed deficit lower than the baseline setup, whose difference to B1 ranges from around 5 % for S2 and S3 to almost 10 % for S1. The wake deficit of B1 increases over the wind farm length by around 8 %, which is stronger compared to the wake deficit of S1 to S3, which increase by around 1 % to 5 %. Especially S1 stands out, with a comparably constant wake deficit of around 90 % of the inflow wind speed along the wind farm length. The smaller deficit of the vertical staggering setups is mainly related to the lower turbine density at 150 m. Still, for S1 calculating the deficit only for the turbines' columns with hub height at 150 m in a y interval $\pm 0.5 s_y$ around the turbines rotor centre, shows a smaller deficit for S1 compared to B1, indicating a better wind speed recovery between the turbine columns, which is discussed in Sect. 3.1.3.

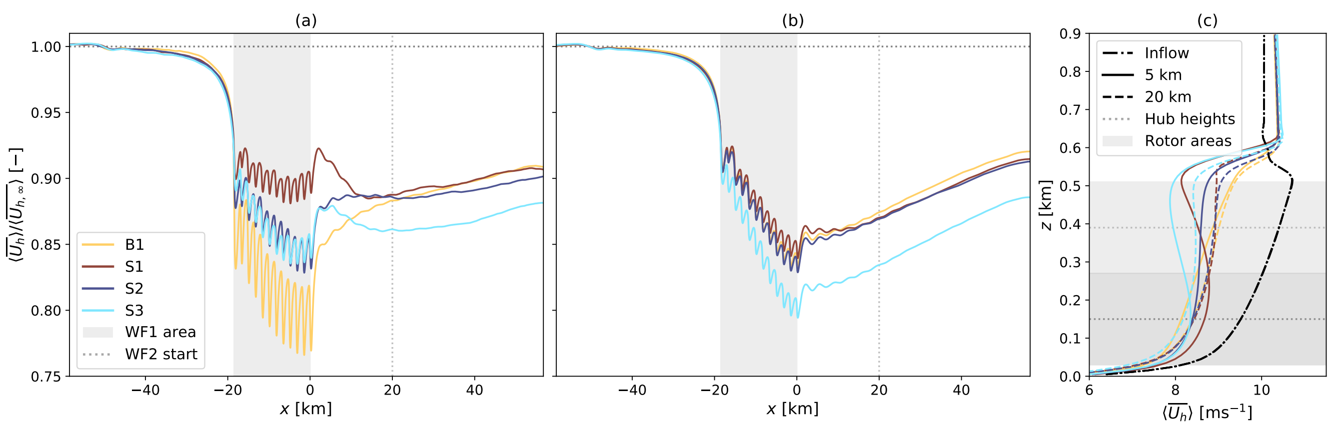

Figure 4. Horizontal wind speed averaged over the full wind farm (WF) width. (a) At the baseline hub height 150 m normalised against the inflow and plotted along the streamwise direction, where x is the distance behind the wind farm. (b) Averaged over the rotor height of the tallest wind farm (vertical average from 30 m to 510 m), normalised against the inflow and plotted along x. (c) As a vertical profile for two locations, 5 km behind the wind farm and 20 km behind the wind farm (start of potential second wind farm (WF2)).

Behind the wind farm at baseline hub height, the wind speed deficit along the streamwise direction suggests a different development and intensity of the wake recovery across the simulated cases (Fig. 4(a)). B1 shows the typical logarithmic wake recovery in streamwise direction. The vertical staggering setups shows a different development in the first 20 km behind the wind farm. The strong increase in wind speed in the first 2 km ($\approx 8D$) is similar to B1. Further downstream, the mean wind speed decreases again for the two setups without overlapping rotor areas (S1 and S3), and to a lesser extent also S2. This decrease in wind speed continues up to 15 km-20 km behind the wind farm. Beyond these distances, the recovery rate is mostly similar to B1.

Since vertically staggered wind farms cause wind speed deficits at multiple heights, analysing only the baseline hub height does not give sufficient insights into the entire wake area. By averaging for all setups the wind speed deficit over the maximum vertical wind farm extent, we can analyse how much momentum each setup extracts in the same volume (Fig. 4(b)). Inside the wind farm area, S2 and S3 have a similarly strong or stronger deficit compared to B1, differing by up to 3 % for S3. S1 has a weaker deficit throughout the wind farm by up to 1.5 %. In the wake downstream of the wind farm, differences in the recovery mainly exist in the first 15 km, where the recovery of S1 is slower compared to B1 and the other vertical staggering setups. Consequently, the downstream deficit of S1 becomes stronger compared to B1.

To analyse the mean vertical wake structure we compare vertical profiles which were averaged over the wind farm width at two distances downstream of the wind farm. At 5 km behind the wind farm, the vertical profiles of the different setups show larger differences by up to 1.5 ms^{-1}, which diminish up to 20 km (Fig. 4(c)). At 5 km, the profiles can be grouped together into three different groups. B1 shows a continuously increasing wind speed up to the CI. The profile of S2 has a more constant wind speed over the boundary layer. The vertical staggering setups without overlapping rotor areas S1 and S3 show a different vertical profile shape, where the wind speed reaches a local minimum inside the rotor area of the higher turbine, close to the upper tip of the rotor. The wind speed at higher altitudes is thus partly smaller than at lower altitudes. In this region, the wind speed is smaller for S3 compared to S1. At 20 km, the minimum in the upper rotor area mostly disappears, resulting for all setups in a monotonous, logarithmic-like increase in wind speed with height. In the following Sect. 3.1.2 we address how the inverted wind profile of S1 and S3 relates to the described mean wind speed reduction at 150 m hub height.

3.1.2 Wake recovery budget

To understand the origin of the described wake differences we calculate the wake recovery budgets. The wake recovery budgets (Fig. 5, Fig. 6) give insight into the factors that influence the gradient of the streamwise wind speed component u in streamwise direction $-\partial_x \overline{u}$, which is an indicator for the streamwise wake recovery and will in the following be referred to as the (streamwise) recovery term $\mathcal{R}$.

With the exception of $\mathcal{R}$, all terms that are positive contribute to wake recovery and negative terms hinder the wake recovery. The largest and therefore most relevant terms are the momentum advection terms $\mathcal{A}_{y,z}$, vertical turbulent momentum flux $\mathcal{T}_z$,

https://doi.org/10.5194/wes-2026-140
Preprint. Discussion started: 10 September 2026

perturbation pressure $\mathcal{P}^*$, and geostrophic pressure term $\mathcal{P}_g$. The horizontal turbulent fluxes $\mathcal{T}_{x,y}$ and Coriolis term $\mathcal{C}$ are small. The drivers of the undisturbed flow which balance each other out in the inflow are the geostrophic pressure gradient $\mathcal{P}_g$ and the vertical turbulent flux $\mathcal{T}_z$ related to the surface friction influencing the logarithmic wind profile.

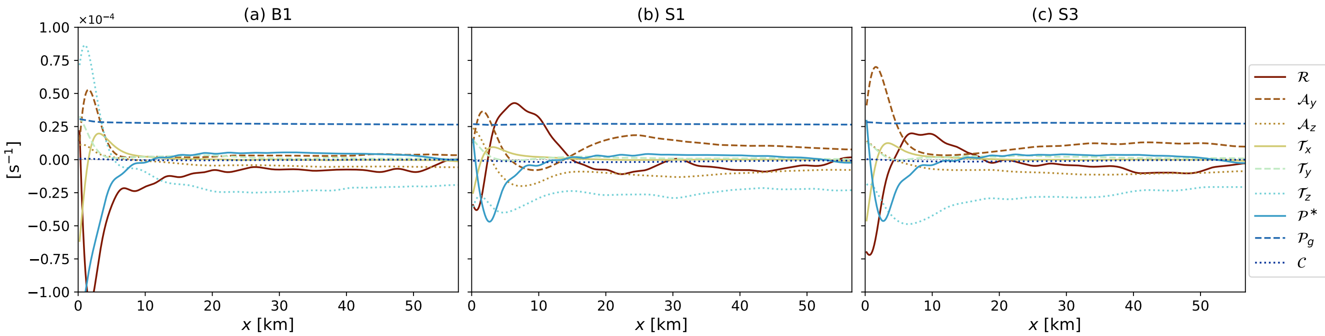

Figure 5. Wake recovery budget along x at 150 m hub height for (a) B1, (b) S1, and (c) S3. Positive values of the budget terms indicate a contribution to the recovery and negative values a hindrance to the recovery. The terms are: recovery $\mathcal{R}$, advection $\mathcal{A}_{y,z}$, turbulent fluxes $\mathcal{T}_{x,y,z}$, perturbation pressure $\mathcal{P}^*$, geostrophic pressure $\mathcal{P}_g$ and Coriolis $\mathcal{C}$.

The streamwise recovery term $\mathcal{R}$ follows the wake recovery development illustrated in Fig. 4(a). For B1 the wind speed recovers continuously over the entire streamwise distance, as indicated by a strongly negative recovery term $\mathcal{R}$, which slowly approaches zero. For S1 and S3 directly behind the wind farm the recovery term is negative, similar to B1. Between 5 km to around 15 km the recovery term approaches values that are close to zero or positive (Fig. 5(b,c)), which relates to the strengthening of the wind speed deficit in the wake shown in Fig. 4(a).

The dominating recovery terms differ depending on the location behind the wind farm. For B1 we can distinguish mainly between the near cluster wake, which is characterised by a fast recovery and is for B1 located in the first 5 km to 10 km, and the far cluster wake, which shows a slower recovery and does not recover fully until the domain end. In the first 5 km, in the near cluster wake, the recovery is mainly caused by a positive turbulent vertical momentum flux component $\mathcal{T}_z$ and vertical advection $\mathcal{A}_z$ transporting higher wind speeds to lower altitudes, and a crosswise advection $\mathcal{A}_y$ caused by flow deflection around the wind farm. The crosswise turbulent flux $\mathcal{T}_y$ contributes depending on the crosswise location, fluctuating around zero over the wind farm extent in crosswise direction (Fig. 6). Further downstream, in the far cluster wake, the turbulent vertical flux $\mathcal{T}_z$ decreases to its original negative level of the inflow and the perturbation pressure $\mathcal{P}^*$ and the crosswise momentum advection $\mathcal{A}_y$ at the northern wake boundary (Fig. 6) contribute to the recovery.

Similar to B1, the vertical staggering cases S1 and S3 show in the near cluster wake an initially strong negative recovery term $\mathcal{R}$ that becomes less negative with increasing distance, similar to Fig. 4(a). The magnitude of the budget terms differ

https://doi.org/10.5194/wes-2026-140
Preprint. Discussion started: 10 September 2026

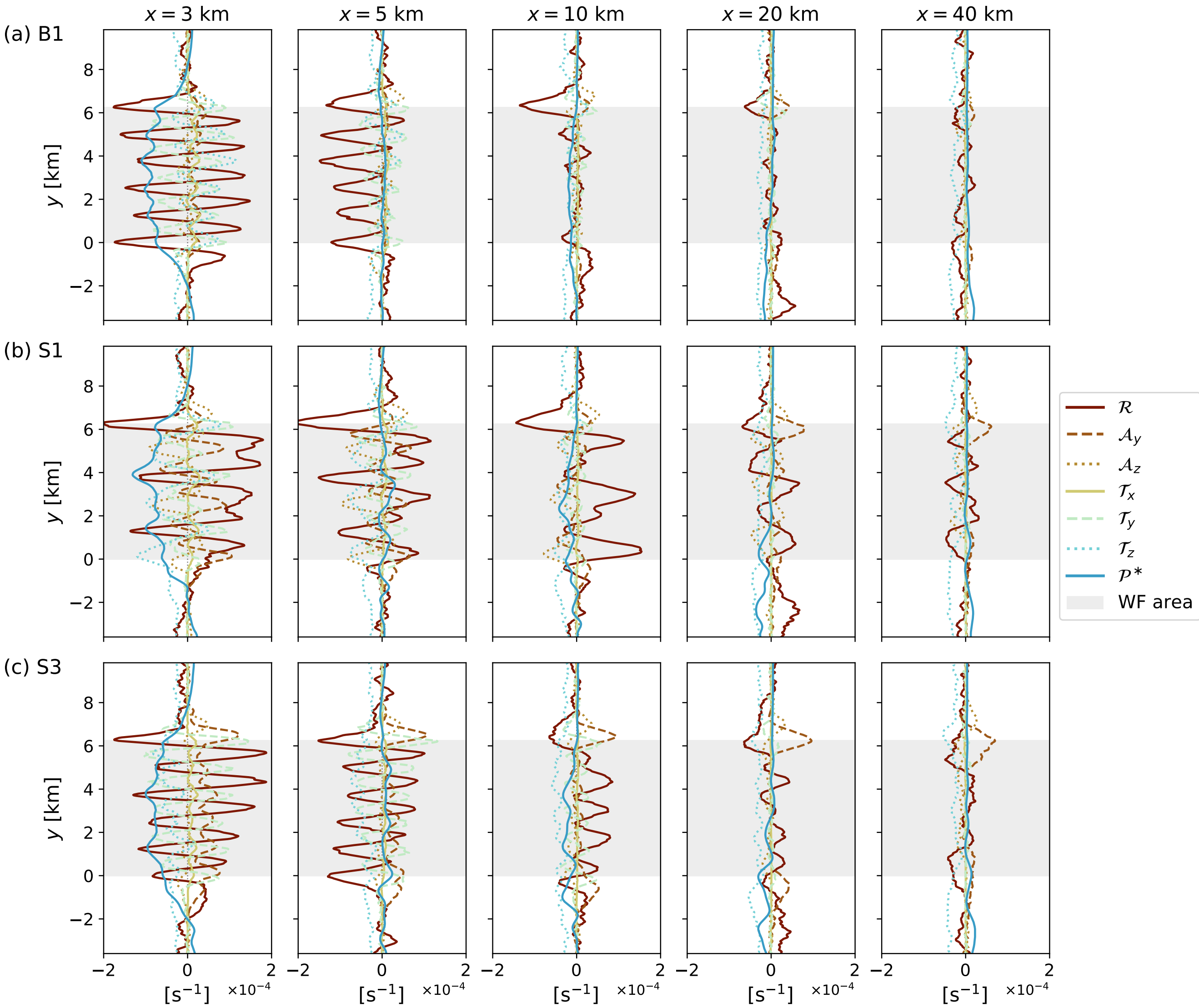

Figure 6. Wake recovery budget along the crosswise direction y at 150 m hub height for (a) B1, (b) S1, and (c) S3 at different locations along the streamwise direction x. The horizontal dotted lines mark the northern and southern boundary of the wind farm. Positive values of the budget terms indicate a contribution to the recovery and negative values a hindrance to the recovery. Some budget terms were excluded from this plot, since they were at maximum in the order of 10^{-6} and thus negligible. The terms are: recovery $\mathcal{R}$, advection $\mathcal{A}_{y,z}$, turbulent fluxes $\mathcal{T}_{x,y,z}$ and perturbation pressure $\mathcal{P}^*$.

between the setups. Compared to B1, both vertical staggering cases show in the first 5 km a less negative recovery term because of a negative turbulent vertical flux term $\mathcal{T}_z$. The negative turbulent flux term is related to the larger wind speed deficit at higher altitudes (Fig. 4(c)). The recovery term is still more favourable for S3 compared to S1 due to a more positive crosswise

https://doi.org/10.5194/wes-2026-140
Preprint. Discussion started: 10 September 2026

and vertical advection term $\mathcal{A}_{y,z}$ entraining momentum from the sides and from higher altitudes. These advection terms are related to the presence of a circulation zone at the northern wake boundary, which are addressed in Sect. 3.1.3. Beyond 20 km downstream, differences between B1 and the vertical staggering cases mainly exist in the crosswise advection term $\mathcal{A}_y$. For B1 this term is comparably small, while for the vertical staggering cases it has a two to four times larger contribution (Fig. 5). The inward transport of momentum is especially strong at the northern boundary (Fig. 6), where a speed-up region is located next to the wake (Fig. 7(b)). The combination of a stronger inward advection and a stronger speed-up region for the vertical staggering cases results in the more positive crosswise advection term $\mathcal{A}_y$. Apart from that, the vertical turbulent and advective terms $\mathcal{T}_z$ and $\mathcal{A}_z$ are more negative for S1 and S3, due to the stronger wind speed reduction at higher altitudes. The cause of the vertical and crosswise advection is further addressed in the analysis of the 3D-flow field in Sect. 3.1.3.

For the vertical staggering cases we already pointed out a third region between 5 km to 15 km with an unfavourable, positive recovery term $\mathcal{R}$, which we define as the so-called intermediate cluster wake. This region is characterised by a more negative turbulent vertical flux $\mathcal{T}_z$ and negative vertical momentum advection $\mathcal{A}_z$. These two terms indicate respectively a turbulent momentum transport from lower to higher altitudes and a downward advection of lower wind speeds from higher altitudes to 150 m baseline hub height, thus hindering the recovery and further strengthening the deficit of the streamwise velocity component u. As described in Fig. 4(c), these lower wind speeds are created behind the turbines with increased hub heights. Comparing S1 to S3 shows a stronger negative vertical advection $\mathcal{A}_z$ for S1, resulting in a more positive, unfavourable recovery $\mathcal{R}$. For S3 the downward advection of low momentum is present across most of the wind farm width, while S1 shows three distinct regions of positive streamwise advection and the related downward advection (Fig. 6). In these regions, we also see a contribution of the crosswise advection $\mathcal{A}_y$ to a strengthening of the deficit (Fig. 6). These spatial differences are further analysed in Sect. 3.1.3.

3.1.3 Three-dimensional flow structures

The average wind speed deficits gave a first indication of differences between vertically staggered and non-staggered wind farms. To understand these differences we characterise the spatial wake structure and three-dimensional flow field. Since the strongest influence on the wake seems to be present for S1, we focus on this setup. To have a comparison with a setup with the same number of turbines per height, we additionally analyse S3. The other setups are only partly referred to.

Horizontal slices of the wind speed at 150 m hub height reveal strong differences in the horizontal wake structure for S1 and B1 (Fig. 7). For B1 (Fig. 7(a)), in the first 20 km downstream of the wind farm, streaks with lower wind speeds behind the six wind turbine columns are visible, while further downstream the wake is mostly homogeneous. Contrary, S1 (Fig. 7(b)) has a more heterogeneous wake with multiple streaks of decreased and increased wind speeds, which persist up to the domain end 60 km downstream. From the 8th turbine row to 10 km downstream of the wind farm three streaks of increased wind speeds are present between the columns with high hub height wind turbines in the south and the columns with low hub height wind turbines in the north. These streaks with increased wind speeds are only present in the lower turbine's rotor area. At

https://doi.org/10.5194/wes-2026-140
Preprint. Discussion started: 10 September 2026

higher altitudes the wind speed is overall decreased, although still heterogeneous with differently strong deficits over the wake width (Fig. 8). The streaks are created by downward advection of higher wind speeds inside the wind farm, as identified in the momentum budget in these speed-up regions.

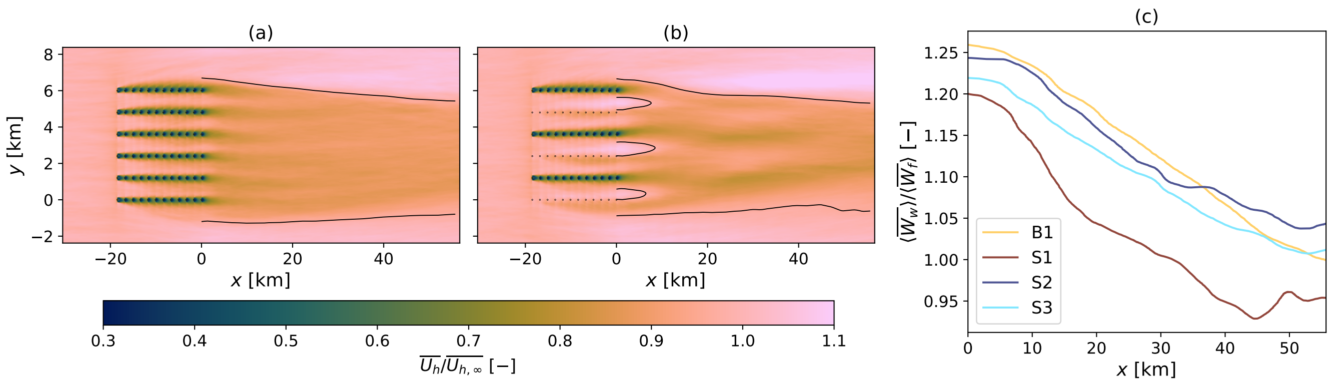

Figure 7. Slice of the horizontal wind speed at 150 m for (a) baseline setup B1 and (b) vertical staggering column setup S1. (c) The wake width W_w is plotted relative to the wind farm width W_f over x for all setups. The solid black lines in (a) and (b) mark the northern and southern wake edges, which were used to calculate the wake width.

The downward advection is related to the formation and presence of three circulation zones (Fig. 8) inside the wind farm of S1 and S2. The circulation zones formed between one column of high turbines and one column of low turbines (Fig. 8(b,e)). The intensity of the circulation zones is defined as the change in magnitude of v and w compared to the undisturbed inflow. The circulation zones thus do not represent the absolute flow, but the flow field change imposed on the background flow which is subjected to wind shear and veer. The three circulation zones start to form inside the wind farm, being visible after the seventh turbine row (Fig. 8(b)), and strengthen towards the end of the wind farm. Behind the wind farm they weaken but still exist more than 20 km downstream of the wind farm (Fig. 8(h)). The vertical motion of the circulation zones advect air with different properties, thus affecting the wake recovery. Depending on the wind profile, this can either increase wind speeds, as seen inside the wind farm and in the first 5 km downstream, or decrease wind speeds, as seen from 5 km to 15 km in the wake of the setups without overlapping rotor areas (Fig. 6).

One feature in the horizontal flow field (Fig. 7) that is present for both, B1 and S1 (as well as S2 and S3), is a speed-up region at the northern wake edge with velocities up to 10 % higher than the inflow wind speed for S1 and up to 5 % higher for B1. The lateral extent of the speed-up region increases with streamwise distance, reaching a few hundred metres for B1 up to almost 2 km for S1. One of the main contributors to this speed-up is the downward advection of air with higher wind speeds (Fig. 6), which is related to the presence of a circulation zone at the northern wake boundary (Fig. 8(f-i)).

https://doi.org/10.5194/wes-2026-140
Preprint. Discussion started: 10 September 2026

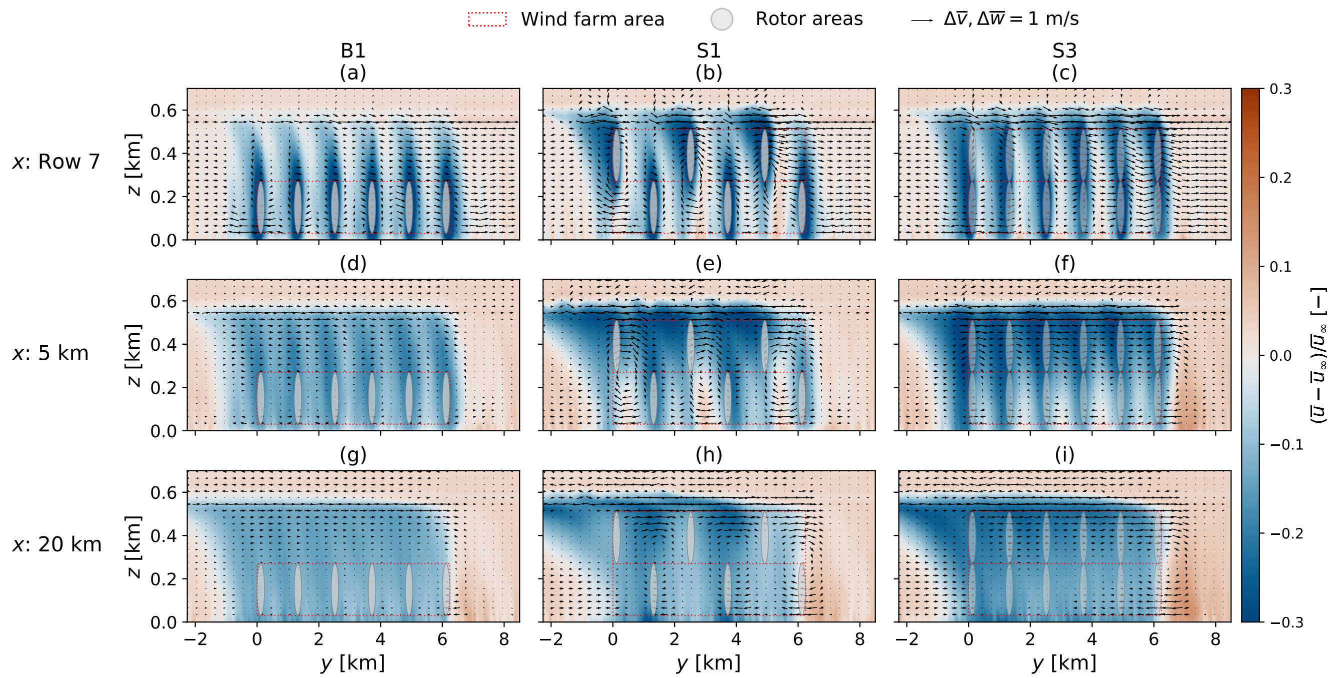

Figure 8. Vertical cross sections (looking upstream) of the normalised difference in the streamwise wind speed component $(\overline{u} - \overline{u}_\infty)/\overline{u}_\infty$ compared to the inflow for (a,d,g) B1, (b,e,h) S1, and (c,f,i) S3 at locations (a,b,c) between the seventh and eighth row of the wind farm, (d,e,f) 5 km downstream, and (g,h,i) 20 km downstream of the wind farm. The arrows depict the difference of the crosswise and vertical wind speed components with respect to the inflow $\Delta\overline{v} = \overline{v} - \overline{v}_\infty$ and $\Delta\overline{w} = \overline{w} - \overline{w}_\infty$.

At the northern wake boundary a circulation zone forms on top of the background flow field in all simulated setups (Fig. 8). To be specific, on the northern hemisphere this zone appears on the left side of the wake, viewed from above in streamwise direction, and on the southern hemisphere on the right side of the wake, as an additional simulation shows. So, to generalise it can be said that the circulation zone appears at the side of the wake the Coriolis force is acting from. Since we simulate westerly flow in the northern hemisphere, the left wake side translates to the northern wake boundary. Looking upstream, this circulation zone has a clockwise rotation direction (Fig. 8). On the southern hemisphere the rotation direction would be opposite. For the different wind farm setups, the circulation zone forms at different streamwise distances, occurring earlier for the vertical staggering setups compared to B1. These differences might be related to the vertical wake extent and the wake intensity close to the CI. For B1, the vertical wake extent still develops downstream of the wind farm with smaller intensities at higher altitudes resulting in a visible circulation zone being present only after 10 km (Fig. 8(g)). For S3, the closeness of the taller turbines to the CI results directly behind the wind farm in the wake to reach up to the boundary layer top and therefore the formation of the circulation zone (Fig. 8(f)). For the setups with alternating columns of low and high turbines S1 and S2, the exact formation of the northern circulation zone is more difficult to define, since already inside the wind farm three circulation zones form, which move northward in the wake downstream of the wind farm (Fig. 8(b,e,h)). The northern circulation zone therefore does not form separately but the northernmost of the three circulation zones shifts to the wake edge and increases in intensity.

To compare the wake extent in crosswise direction, we calculate the wake width from the difference between the wake boundaries, which are defined as 97 % of the inflow wind speed at baseline hub height (Fig. 7(c)). The wake width of all vertical staggering setups is smaller compared to B1. At the end of the wind farm, the wake width of B1 is around 126 % of the wind farm width, while for the vertical staggering setups it ranges between 120 % to 125 %. For B1, the wake width narrows down constantly by around 5 % of the wind farm width (≈ 0.3 km) per 10 km streamwise distance (Fig. 7(c)). For S1, the wake width decreases faster in the first 20 km by around 10 % of the wind farm width (≈ 0.6 km) per 10 km streamwise distance (Fig. 7(c)). This results in a difference in wake width between B1 and S1 of up to 15 % of the wind farm width (≈ 1 km). Comparing the wake width for the other vertical staggering setups shows generally a narrower wake by up to 5 % of the wind farm width (≈ 0.5 km) compared to B1 (Fig. 7(c)). This difference is mostly present up until the domain end.

The wake width differences can mainly be explained by crosswise momentum advection at the northern wake boundary and for S1 also by the direct influence of the column setup. For S1, the smaller wake width is mainly related to the southernmost turbine row being located at 390 m hub height. This row causes at 150 m height a comparably weaker deficit that reaches less far south compared to the other setups (Fig. 8(e)). For all the other setups, the main contributor to the narrower wake is a stronger crosswise advection due to a more negative crosswise wind speed component $\overline{v}$ and the stronger speed-up region in the free stream. Note that these mechanisms are relevant for the wake width at baseline hub height, while at higher altitude the wake width might be differently affected. Vertical slices show that the wake at higher altitudes expands in lateral direction, especially at the southern boundary (Fig. 8), which can be related to a clockwise wake deflection and larger northern wind direction component.

The crosswise advection and thus the wake narrowing is related to a circulation zone at the northern wake boundary. Depending on the distance at which the circulation cell forms and eventually decays, the wake width changes differently strong. This is especially the case for S3, where the circulation zone already forms directly behind the wind farm and strengthens until around 30 km (Fig. 8(f,i)), causing the stronger wake narrowing compared to the baseline setup, for which the circulation is weaker and increases less in intensity until around 20 km.

3.2 Influence of vertical staggering on the wake of a downstream wind farm

Since we found considerable differences in the wake characteristics of vertically staggered and non-staggered wind farms, a second wind farm located downstream might be impacted differently according to the turbine arrangement of the upstream wind farm. To test this hypothesis, we analyse the internal and external wake of a second, non-staggered wind farm WF2, which is located 20 km downstream of WF1. As shown in Fig. 4(a), at this distance the mean wake at hub height is differently strong but recovers with a similar rate for all setups. The wake heterogeneities and smaller wake deficit at high altitudes still

https://doi.org/10.5194/wes-2026-140
Preprint. Discussion started: 10 September 2026

exist for the vertical staggering setups.

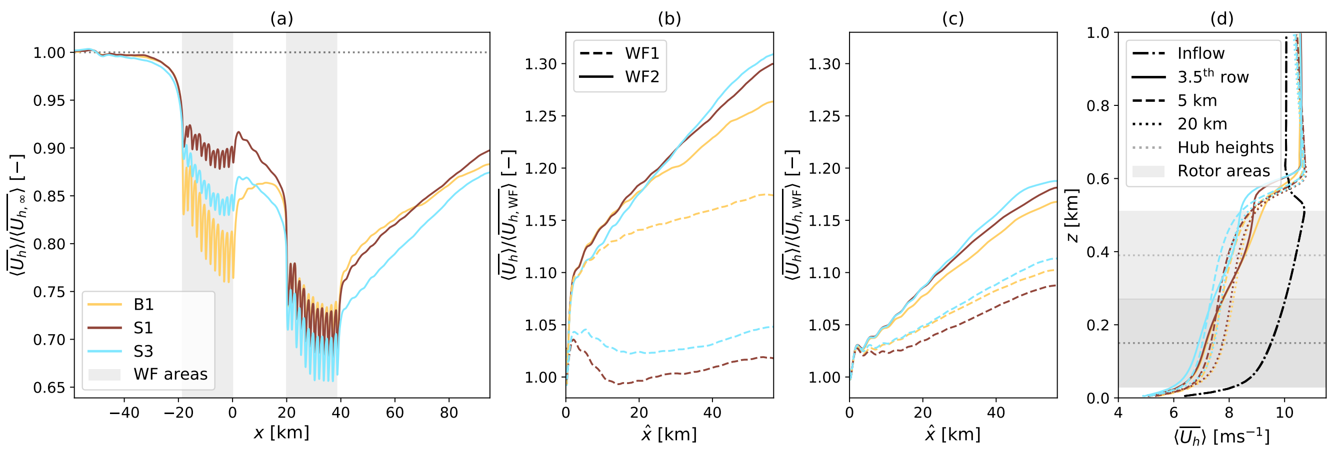

Figure 9. Horizontal wind speed averaged over the full wind farm (WF) width. (a) At 150 m height, normalised against the inflow and plotted along the streamwise direction, where x is the distance behind the upstream wind farm. (b) At 150 m height, normalised against the wind speed $1.5D$ behind the last row of the wind farm, where $\hat{x}$ is the distance behind the upstream wind farm (WF1 without WF2, dotted) or the downstream wind farm (WF2, solid). (c) Similar as (b), but averaged over the maximum vertical wind farm extent (30 m to 510 m). (d) As vertical profiles for three locations: between the third and fourth turbine row, and 5 km and 20 km behind the downstream wind farm.

In the first half of the downstream wind farm WF2, the mean inner wind farm wake is comparable for B1 and S1 at a height of 150 m (Fig. 9(a)), despite the higher wind speed in the inflow of S1 (Fig. 4(a)). In the second half of WF2, the deficit of B1 is mostly constant, while the deficit of S1 strengthens further, resulting in a 2 % stronger wake deficit at the end of WF2. Vertical slices inside the downstream wind farm reveal that the wake deficit at higher altitudes is still heterogeneous and partially stronger for S1 compared to B1, differing by up to ≈10 % of the inflow (Fig. 10(a,c)). For S3, the inner wake is stronger throughout the wind farm (Fig. 9(a)), which can be related to the stronger deficit at higher altitudes (Fig. 9(d)) and partially results in a stronger wind speed deficit between the turbine columns (Fig. 10(a-c)).

The three circulation zones that are present in the wake of the upstream staggered wind farm S1 are strongly affected by the wind turbines of WF2. Within the first few rows of WF2, the circulation zones break down. At turbine height this happens at the start of WF2 due to the direct influence of the turbines and their wakes. Above the wind farm, the remains of the circulation zones are broken down as soon as the individual wakes vertically spread to higher altitudes, which happens around the third and fourth row (Fig. 10(b)). Since the vertical motion of the circulation zones is still present inside the wind farm, the internal wake properties are influenced. In this case, this means that at these locations the wind speed between the turbine columns is higher compared to the baseline setup (Fig. 10(a,b)). However, this result depends on the location of the vertical advection with

https://doi.org/10.5194/wes-2026-140
Preprint. Discussion started: 10 September 2026

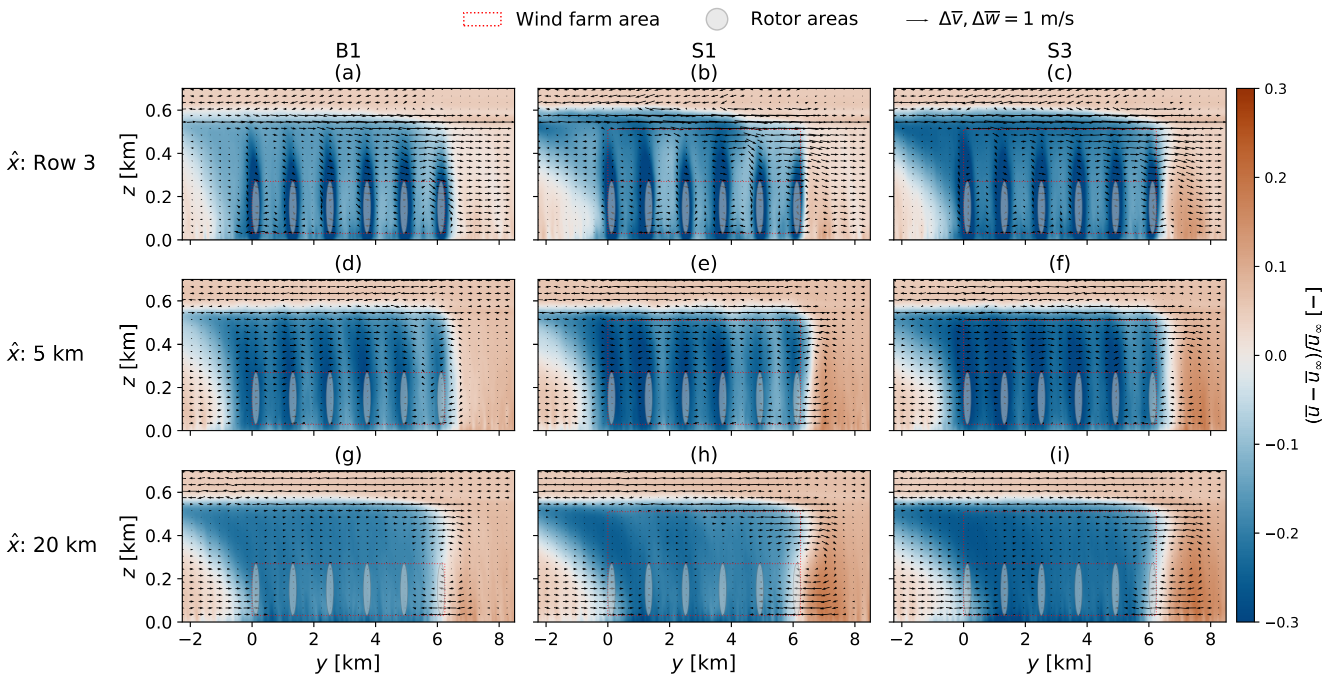

Figure 10. Vertical cross sections (looking upstream) of the normalised difference in the streamwise wind speed component $(\overline{u}-\overline{u}_\infty)/\overline{u}_\infty$ compared to the inflow for (a,d,g) B1, (b,e,h) S1, and (c,f,i) S3 inside and downstream of WF2, at locations (a,b,c) between the third and fourth turbine row, (d,e,f) 5 km downstream of WF2, and (g,h,i) 20 km downstream of WF2. The arrows depict the difference of the crosswise and vertical wind speed components compared to the inflow $\Delta\overline{v}=\overline{v}-\overline{v}_\infty$ and $\Delta\overline{w}=\overline{w}-\overline{w}_\infty$.

respect to the streaks of higher or lower wind speeds at high altitudes.

Compared to the deficit behind the single upstream wind farm WF1 of around 80% to 90%, the wake deficit behind the downstream wind farm WF2 is stronger with 70% to 75% (Fig. 9(a)). Comparing the rate of the wake recovery between the single upstream wind farm and the downstream wind farm shows for the downstream wind farm a faster recovery rate in all cases at hub height (Fig. 9(b)) and averaged over the maximum vertical wind farm extent (Fig. 9(c)), resulting in large differences in the wake deficit between WF1 and WF2. At 150 m hub height (Fig. 9(b)), the largest differences in the recovery rate start for B1 downstream of 10 km behind the wind farm, having a recovery rate of 2.5 %/km behind the downstream wind farm compared to 0.8 %/km behind the upstream wind farm. This results for B1 in an absolute deficit difference by almost 10 % at the end of the domain (Fig. 9(b)). For the vertical staggering cases the recovery rate is faster compared to the upstream wind farm already after 5 km, since the wake at 150 m height of the upstream staggered wind farm barely recovers due to the decreased wind speeds at higher altitudes, which is not the case for the non-staggered downstream wind farm. This results for the vertically staggered wind farms in absolute deficit differences by up to 30 % at the end of the domain. The faster recovery of the downstream wind farm's cluster wake at 150 m height can in all cases be explained by a larger crosswise advection

https://doi.org/10.5194/wes-2026-140
Preprint. Discussion started: 10 September 2026

(Fig. 11), which is downstream of 30 km up to two to three times larger compared to the upstream wind farm (Fig. 5) and has now also a relevant contribution at the southern wake boundary. At the northern boundary, this stronger crosswise advection is related to the circulation zone, which increases in intensity compared to the wake of the upstream wind farm for all three setups (Fig. 10). For S1 and S3, the less negative turbulent vertical momentum flux and vertical advection in the first 10 km to 15 km behind the non-staggered downstream wind farm additionally contributes to less hindrance of the recovery compared to the upstream, staggered wind farm (Fig. 11).

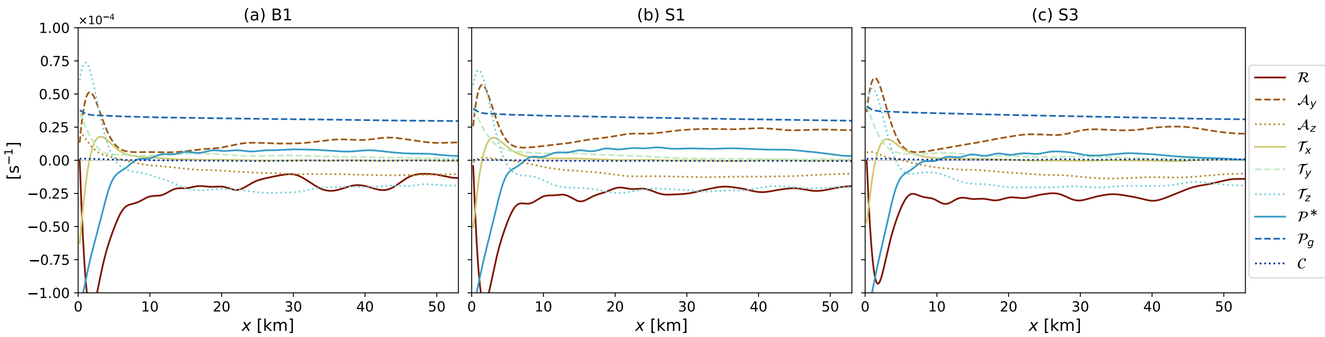

Figure 11. Wake recovery budget behind the downstream wind farm WF2 along x at 150 m hub height for (a) B1, (b) S1, and (c) S3. Here, $x = 0$ marks the end of the downstream wind farm. Positive values of the budget terms indicate a contribution to the recovery and negative values a hindrance to the recovery. The terms are: recovery $\mathcal{R}$, advection $\mathcal{A}_{y,z}$, turbulent fluxes $\mathcal{T}_{x,y,z}$, perturbation pressure $\mathcal{P}^*$, geostrophic pressure $\mathcal{P}_g$ and Coriolis $\mathcal{C}$.

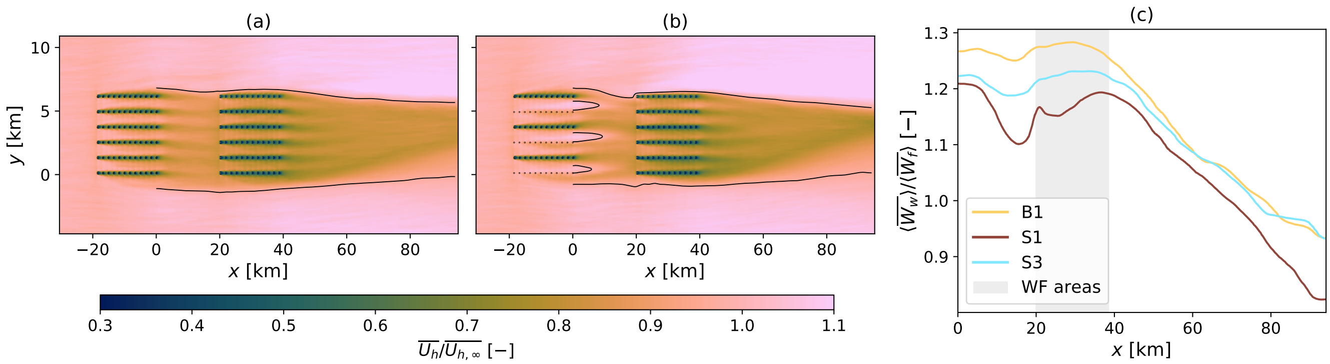

Figure 12. Slice of the horizontal wind speed at 150 m for (a) baseline setup B1 and (b) vertical staggering column setup S1. (c) The wake width W_w is plotted relative to the wind farm width W_f over x. The solid black lines in (a) and (b) mark the northern and southern wake edges, which were used to calculate the wake width.

https://doi.org/10.5194/wes-2026-140
Preprint. Discussion started: 10 September 2026

eawe european academy of wind energy
Open Access WIND ENERGY SCIENCE DISCUSSIONS

490 The observed differences in the wake width can be explained by differing intensities of the northern circulation zone. The wake width is smaller for the vertical staggering cases compared to B1, being narrower for S1 compared to S3. This is similar to the wake width behind the upstream wind farm (Fig. 7), although the differences are overall smaller by a maximum of 5 % of the wind farm width. The narrowing rate is mostly similar for all setups, with some local variations and a slower narrowing of the wake of S1 in the first 10 km behind the wind farm. Comparing the wake width behind the downstream wind farm
495 (Fig. 12) to the wake with behind the upstream wind farm (Fig. 7) shows a faster narrowing for B1 and S3, which is related to the stronger crosswise advection at the northern and southern boundary. For S1, the crosswise advection at the downstream wind farm is also stronger, but since the effective wind farm width at 150 m is wider for the non-staggered downstream wind farm, the net wake narrowing happens slower compared to the upstream wind farm (Sect. 3.1.3).

3.3 Power production differences in the upstream and downstream wind farm

500 The difference in the total power production of the upstream wind farm, the downstream wind farm and the sum of both wind farms with respect to B1 is summarised in Table 2. For the upstream wind farm, the staggered setups produce more power than B1, with an increase by 19.1 % for S1 and 45.3 % for S3, showing an increased power production in each row of the wind farm (Fig. 13(a)). Comparing the total power production to the wind speed deficit over the maximum wind farm height (Fig. 4(b)) we see as expected that S3, the setup with the largest power production has the strongest wake deficit, while B1 has a smaller
505 power production and thus a smaller deficit. In contrast, S1 shows the smallest deficit at the end of the wind farm (Fig. 4(b)), while producing more power than B1. This indicates more momentum entrainment from outside the averaging area.

Table 2. Power production change of WF1, WF2, and both wind farms combined for all setups normalised by the respective wind farm of B1 ($\Delta P = (P_{\mathrm{S}_i} - P_{\mathrm{B1}})/P_{\mathrm{B1}} \cdot 100$).

	B1	B2	S1	S3
WF1	±0 %	+27.8 %	+19.1 %	+45.3 %
WF2	±0 %	+2.7 %	+0.9 %	−11.8 %
Total	±0 %	+17.3 %	+11.5 %	+21.5 %

The increased power of the vertically staggered wind farms can be mainly attributed to the higher inflow wind speeds for the taller turbines (Fig. 13(b,c)), a lower turbine density per height, and the internal wake recovery. The staggering setup of S3 resembles a horizontally staggered wind farm at both hub heights, while S1 resembles an aligned setup with wider column
510 spacing. The higher power production of S3 compared to S1 can be attributed to this horizontally staggered setup. Especially the second row created more power since it receives the undisturbed inflow, and the following rows receive higher wind speeds due to the effective larger turbine-spacing in streamwise direction (Fig. 13(c)).

Spatial differences in the power production within the wind farm exist. For S1 some of the lower turbines produce less power
515 compared to the baseline setup, mainly in the first one to three rows and some turbines of the southernmost low turbine column.

https://doi.org/10.5194/wes-2026-140
Preprint. Discussion started: 10 September 2026

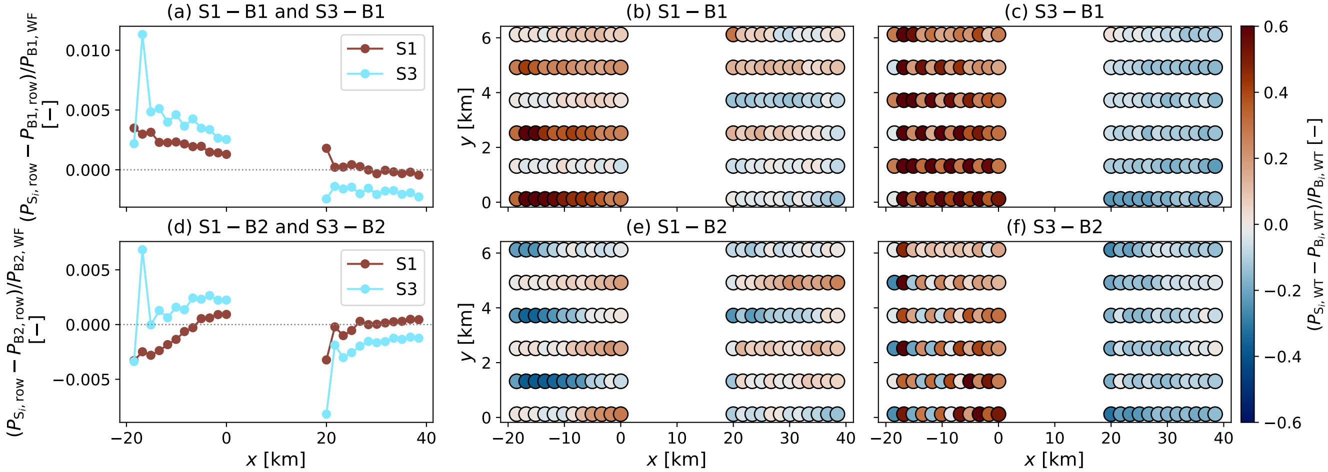

Figure 13. Power production of S1 and S3 compared to B1 and B2. (a,d) Difference in the average power per row between the vertical staggering setup S_i and the baseline setup B1 (a) or B2 (d), normalised with the power production of the total wind farm. (b,c,e,f) Difference in the turbine power between the vertical staggering setup S1 (b,e) or S3 (c,f) and the baseline setup B1 (b,c) or B2 (e,f), normalised against the respective turbine of B1 or B2.

The lower power production in the southernmost row of S1 is likely related to the downward transport of lower wind speeds, since at this location the wake at higher altitudes already developed to have lower wind speed than at lower altitudes. For S3 we similarly observe a power decrease of the low turbines in the first row. The lower power production in the first row(s) can be associated to the increased blockage mentioned in Sect. 3.1.1. In the two northern low turbine rows of S1, the power production in the second half of the wind farm is larger than B1, which can be explained by the streaks of increased wind speeds at lower altitudes (Fig. 7).

To assess which of the described factors are most relevant for a power increase, we performed a second baseline run B2, where all turbines of the upstream wind farm are put to the non-overlapping hub height of 390 m (Tab. 1). Both vertical staggering setups show throughout the wind farm an increasing power production relative to B2, where the second half of the wind farm has on average a larger power production than B2 (Fig. 13(d)). This indicates that with increasing distance inside the wind farm, turbines benefit more from the lower turbine density and improved internal wake recovery, which is for both the shorter and taller turbines the case. In the first half of the wind farm of S1, the increased wind speeds are more relevant, as S1 and B2 have a similar power production of the tall turbines. For S3, the power production in the first half of the wind farm is already mostly larger compared to B2 due to the combination of higher wind speeds and lower turbine density, resulting in an overall larger power production by 14.8 % compared to B2.

https://doi.org/10.5194/wes-2026-140
Preprint. Discussion started: 10 September 2026

The total power production of the non-staggered downstream wind farm in case S1 is 0.9 % higher compared to the power production of the downstream wind farm in case B1, while the downstream wind farm of S3 has a significantly smaller power production by 11.8 %. For S1, the first few rows have on average a higher power production, while a decreased power production is mainly present in the last few rows (Fig. 13(a)). Spatially, strong differences exist between the turbine columns with either mostly an increased or decreased power production. These differences between the columns can be associated with the streaks of lower or higher wind speeds in the farm wake (Fig. 7). Depending on the location of these streaks with respect to the turbines of the downstream wind farm, this affects the power production and either results in increased or decreased power production. For S3, the entire downstream wind farm shows a significantly lower power production due to the continuous decreased inflow (Fig. 8), except for a higher power production in few turbines of the northern column (Fig. 13(c)), which can be attributed to the speed-up region at the wake boundary.

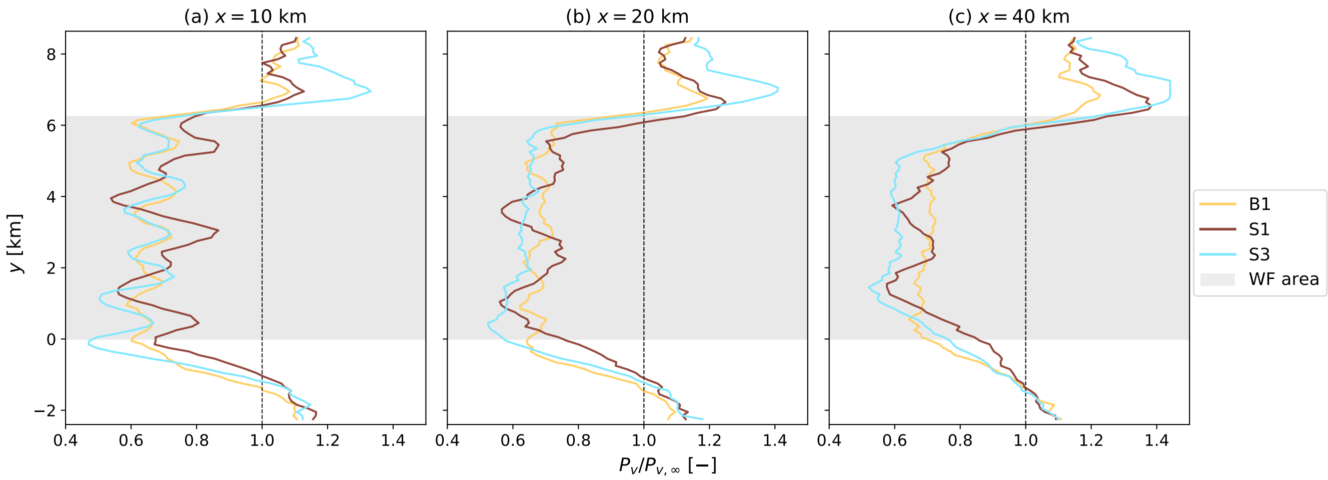

Figure 14. Power production of virtual turbines calculated from the rotor equivalent wind speed and plotted along y at (a) 10 km, (b) 20 km, and (c) 40 km downstream of WF1, normalised against the virtual power calculated in the undisturbed inflow.

Since the wake heterogeneities and speed-up region at the wake boundary vary in streamwise and crosswise direction, it is sensible to analyse more than one location of the downstream wind farm. We can get an indication for such spatial variations by calculating the normalised power of virtual turbines from the rotor equivalent wind speed at different locations in the flow field (Fig. 14). The speed-up region at the northern boundary allows a higher power production for the vertical staggering setups, which is mainly present 0.5 km to 1.5 km north of the wind farm area and becomes more pronounced with increasing distance. At a distance of 10 km downstream of WF1, wake heterogeneities in crosswise direction are relevant for all setups. Further downstream, mainly S1 shows power differences in crosswise direction, which are related to the wake heterogeneities described in Sect. 3.1.3 and aligned with the power differences described in Fig. 13(b).

https://doi.org/10.5194/wes-2026-140
Preprint. Discussion started: 10 September 2026

4 Discussion

4.1 Wake characteristics and recovery mechanisms of vertically staggered wind farms

Our results aim to give insights into whether vertically staggered wind farms could mitigate cluster wakes by analysing how vertical staggering affects the wake recovery mechanisms, wake characteristics and a downstream wind farm. According to previous studies vertically staggered wind farms can be associated with shorter external wakes (Wang et al., 2025) and increased vertical kinetic energy fluxes inside the wind farm (Chamorro et al., 2014). This could lead to the hypothesis, that vertically staggered wind farms can improve wake recovery. However, our results demonstrate that this is not necessarily the case and strongly depends on the staggering setup and local effects.

We found in CNBL simulations that strongly increased hub heights of selected wind turbines reduce the wind speed at higher altitudes to a degree that smaller wind speeds are advected downwards, inhibiting the wake recovery or even strengthening the deficit at lower altitudes. The hindering of the wake recovery depends on the hub height increase of the taller turbines, as non-overlapping rotor areas result in a stronger wake deficit compared to overlapping rotor areas. The wake deficits at the end of the domain allow conclusions about the wake length since the recovery rate is constant in the last 40 km and can be expected to remain similar. Most vertical staggering setups thus have a larger wake length, which contradicts the study by Wang et al. (2025) describing shorter wake extents for vertically staggered wind farms. Only our column setup without rotor overlap S1 had a smaller wake extent due to stronger momentum advection. The setup by Wang et al. (2025) is more similar to our setup S3 with the longest wake. The differences between our results and the study by Wang et al. (2025) could be related to the differing atmospheric boundary conditions. Wang et al. (2025) simulated an NBL while we set up a CNBL. The presence of a CI and veer can strongly affect wake characteristics, especially for larger wind farms (Lanzilao and Meyers, 2025; Maas and Raasch, 2022).

An increase in vertical kinetic energy flux inside vertically staggered wind farms was described by previous studies as a potentially benefiting factor for the wake recovery of smaller wind turbines with lower hub heights inside a wind farm with larger turbines (Chamorro et al., 2014; Chatterjee and Peet, 2019), although increased turbine size could also result in lower turbines being detached from the undisturbed flow above and thus receive lower wind speeds (Zhang et al., 2018). Our results show that inside the wind farm lower turbines could benefit from a downward transport of higher wind speeds, although in our column staggered case vertical and crosswise advective transport is more important than turbulent transport due to the formation of circulation zones. However, as soon as the wake of the higher turbines develops and the wind speed at higher altitudes overall decreases, the wake recovery is hindered.

The main two wake recovery terms indicated by our momentum budget analysis for the baseline run are the turbulent vertical flux $\mathcal{T}_z$ and crosswise advection $\mathcal{A}_y$, which coincides with the momentum budget results by Lanzilao and Meyers (2025). In their LES study on a non-staggered wind farm, the vertical turbulent flux is the main contributor in the first 5 km of the cluster wake. Similarly, Maas and Raasch (2022) described a positive momentum flux divergence in the near wake, which results in a

https://doi.org/10.5194/wes-2026-140
Preprint. Discussion started: 10 September 2026

fast recovery and becomes negative in the far wake, hindering the wake recovery. How fast the vertical turbulent momentum flux drops after 5 km depends on the closeness of the wind farm top to the capping inversion, since the capping inversion hinders the vertical turbulent entrainment (Lanzilao and Meyers, 2025). This could add to our explanation on why for the vertical staggering cases the vertical turbulent flux becomes more negative already in the first few kilometres of the wake. Since the turbine tips of a vertically staggered wind farm are closer to the capping inversion, the turbulent kinetic energy entrainment could be weaker.

Similar to our results, in the study of Lanzilao and Meyers (2025) the crosswise advection becomes important for the wake recovery beyond 10 km downstream of the wind farm, entraining momentum from the sides. This crosswise advection is less efficient compared to the turbulent vertical flux, since the advection only acts on the wake edge and not the entire wind farm (Lanzilao and Meyers, 2025). However, our vertically staggering setups show that higher wind farm extents with respect to the capping inversion can increase the crosswise advection. Contrary to Lanzilao and Meyers (2025) and our results, Kasper and Stevens (2026) conclude that vertical mechanical energy fluxes, which include vertical advection, dominate farm-scale recovery while crosswise recovery mechanisms, including advection, are negligible. These contrasting conclusions might be related to said wind farm height with respect to the capping inversion, since the LES setup by Kasper and Stevens (2026) was characterised by a deep neutral atmosphere that might allow more vertical transport and thus promote less crosswise flow compared to our shallow neutral atmosphere. Besides advective recovery mechanisms, Maas and Raasch (2022) described that in the far cluster wake mainly the large-scale pressure gradient force drives the wake recovery, together with a counterclockwise deflection of the cluster wake caused by the Coriolis force. This is however mainly relevant for Rossby-numbers around or smaller than 1, which are under the here simulated conditions present for very large wind farms in the order of 100 km. In our cases, the geostrophic pressure gradient related to Coriolis had in the far wake a large contribution, but it was mainly compensated by the vertical momentum flux gradient, similar to the inflow. Overall, our results support the conclusion of Lanzilao and Meyers (2025) and Maas and Raasch (2022) that the vertical turbulent momentum flux is not necessarily the main contributor for the wake recovery at larger distances behind the wind farm, depending on the wind farm setup. For vertically staggered wind farms the advective vertical and crosswise momentum transport can become more important for the wake recovery than the turbulent fluxes.

4.2 Circulation zones and Prandtl's secondary flow

One unexpected result is the formation of circulation zones between a column of high and low turbines (Fig. 15(1)), which are imposed on the flow for the vertical staggering setup with alternating columns of high and low turbines S1 and S2. Fig. 15 provides a graphical summary of the main findings to support the following discussion sections.

Since most studies so far investigated more regular vertical staggering patterns, like the one of S3, the potential of vertically staggered wind farms forming large-scale circulation structures inside the wind farm and wake has to our knowledge not been described in literature yet. However, Chatterjee and Peet (2019) found for their infinite wind farm with added smaller turbines

https://doi.org/10.5194/wes-2026-140
Preprint. Discussion started: 10 September 2026

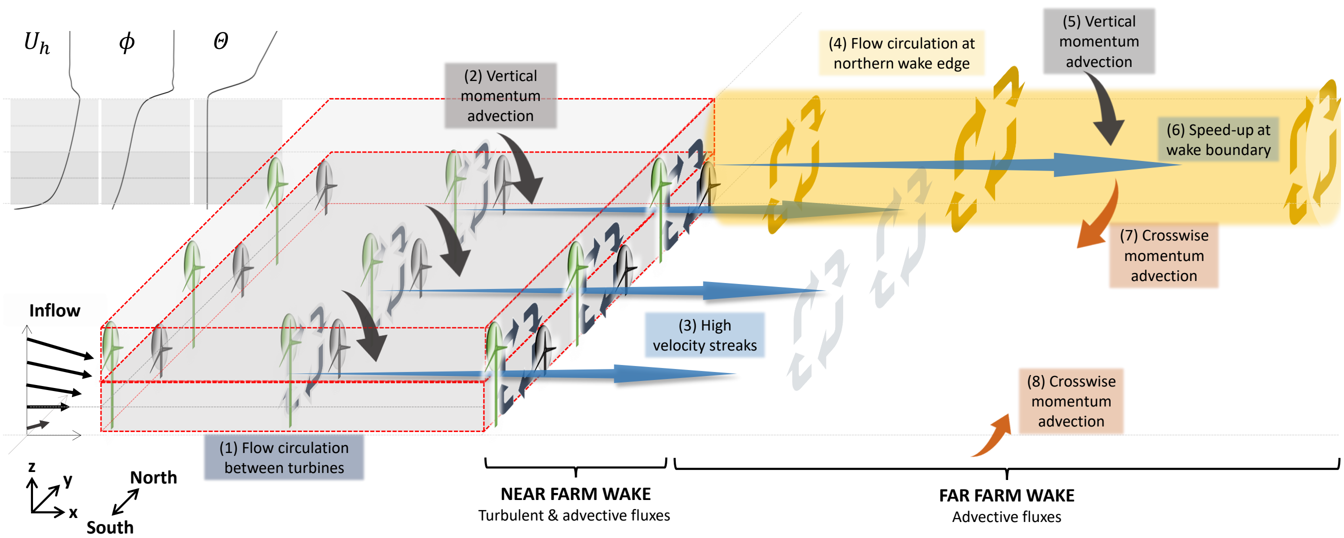

Figure 15. Graphical summary of the main findings. In a CNBL, vertical staggering setups with alternating columns of low and high turbines can create flow circulation (1) that entrains momentum from higher altitudes (2), resulting in high velocity streaks in the lower half of the staggered wind farm (3). For all setups, including a baseline setup, at the northern wake edge flow circulation (4) develops with a stronger magnitude for vertically staggered wind farms with high hub heights. This circulation is associated with vertical momentum advection (5), which creates a speed-up at the wake boundary (6), and crosswise momentum advection (7), which enhances wake recovery and reduces the wake width in the far farm wake. At the southern wake boundary weaker crosswise momentum advection (8) exists without a circulation cell. In the near farm wake, turbulent fluxes are still relevant for wake recovery while in the far farm wake mainly advection is important.

downdrafts of kinetic energy by large-scale flow structures, which were identified in a spectral analysis. Also, the general concept of the formation of circulation zones due to obstacles in the flow were the subject of a few studies. Li et al. (2025) showed in their study that Multi-Rotor Systems with lifting devices can strongly change vertical entrainment and cause circulation zones. Their approach with lifting devices and the underlying physical processes are different to the presented results of vertically staggered wind farms. Yet, it underlines the result that changing the design of the obstacle in the flow, like the wind farm layout, could change flow advection to a degree that in the far cluster wake advection becomes more relevant to wake recovery than turbulent fluxes (Li et al., 2025).

A formation of circulation cells was previously described by studies which investigated the influence of a changed roughness on the flow by placing blocks in a column-like setup on the ground (Anderson et al., 2015; Vanderwel and Ganapathisubramani, 2015). These differences in the surface roughness cause heterogeneities in the TKE distribution along y, similar to our column-staggering setups (S1,S2) (Fig. A2). These studies describe the formation of counter-rotating vortices at the edges of the low and high momentum zones created by the columns. These circulation cells are caused by Reynolds shear and normal stresses and an imbalance in the TKE production and dissipation that result in vertical advection along this turbulence gradient,

https://doi.org/10.5194/wes-2026-140
Preprint. Discussion started: 10 September 2026

eawe european academy of wind energy
Open Access WIND ENERGY SCIENCE DISCUSSIONS

which causes lateral motion to preserve continuity. This flow is referred to as Prandtl's secondary flow of the second kind (Anderson et al., 2015). Since we did not investigate the origin of the circulation cells in this study, it is not possible to say whether the origin is related to secondary flow of the second kind as described by Anderson et al. (2015) and Vanderwel and Ganapathisubramani (2015). However, we can compare our results to their findings to indicate whether the creation of the circulation zones might be related to similar processes. First, we do not describe counter-rotating cells, but singular circulation zones with one rotation direction. In principle, this could still be related to secondary flow if we have a sharp transition of turbulence only between certain turbine pairs, but in Fig. A2 we see that this is not the case inside the wind farm of S1. Second, in our case these circulation zones are not necessarily located at the interface where high TKE neighbours a low TKE, but partly form around the area of increased TKE (Fig. A2). This difference could be explained by the atmospheric conditions under which the secondary flow was investigated by Anderson et al. (2015) and Vanderwel and Ganapathisubramani (2015), being a neutral stratification without a capping inversion, no Coriolis, and thus no veer. If we repeat our simulation S1 without Coriolis and without veer, we get similar results to the ones described in the secondary flow studies, showing counter-rotating vortices around the locations of the increased turbine columns. These results indicate, that inside a CNBL more processes could be relevant for the formation of circulation zones besides secondary flow of the second kind, showing the importance of including veer and Coriolis in a realistic atmospheric flow simulation to understand cluster wakes. These processes responsible for forming flow circulation should be investigated in future studies. Further, our results on the formation of complex flow patterns highlight the importance of using high-resolution models to understand wind farm cluster wake behaviour, especially for more complex, heterogeneous wind farm designs.

4.3 Northern circulation zone

The presented results on the northern circulation zone can give insights into the wake of vertically staggered wind farms as well as non-staggered wind farms. In the northern hemisphere, the circulation zone appears at the left side of the wake (Fig. 15(4)), which seems to be related to a sharp wake edge that reaches up to the capping inversion. At the right side of the wake the wake edge is smeared out over height due to the wind direction change with height, resulting in no circulation zone being present. The circulation strength depends on the capping inversion height with respect to the wind farm height (Lanzilao and Meyers, 2025), where a larger ratio of inversion height to wind farm height results in weaker circulation, and the veering strength inside the atmospheric boundary layer (Centurelli et al., 2025), where a stronger wind direction change with height results in stronger circulation. Thus, in our results vertically staggered wind farms with larger wind farm heights show a stronger circulation zone.

The presence of a circulation zone at the left wake boundary was already described by Lanzilao and Meyers (2025) in LES, mentioning in the upper wake a flow towards the wake edge and a downward flow inside the wind farm area. The location of the downward flow is slightly different to our results, since we found a downward flow next to the wake in the free-stream. This difference could be explained by the differing atmospheric conditions, the wind farm setups and the wind farm height with respect to the boundary layer, since we also found differences in the exact location and extent of the circulation zone between

https://doi.org/10.5194/wes-2026-140
Preprint. Discussion started: 10 September 2026

our baseline and vertical staggering cases and depending on the distance to the wind farm.

A crosswise entrainment into the wake at the lower wake edge is for Lanzilao and Meyers (2025) mainly present at the right edge. We describe a similar lateral entrainment at the right edge of the wake, so the southern wake boundary (Fig. 15(8)). However, we also found lateral entrainment at the left wake edge, related to the circulation zone at that location. Because the lateral entrainment at the left edge was related to a circulation zone that transported faster wind speeds to lower altitudes and eventually laterally into the wake area (Fig. 15(5,7)), it had a bigger contribution to the wake recovery compared to the entrainment at the right edge. The differences in the entrainment at the left edge compared to Lanzilao and Meyers (2025) are related to the strength of the circulation zone. Our vertical staggering setups have a stronger circulation zone, resulting in a stronger crosswise entrainment at the northern wake edge. The circulation zone described by Lanzilao and Meyers (2025) is more similar to our baseline setup, where we also described less lateral entrainment, which is however still directed into the wake.

Since the presence of Coriolis force and veer is relevant for the formation of circulation zones, in other boundary layers the occurrence of circulation zones at the wake edges might differ. Stieren and Stevens (2022) simulated an NBL with small veer and without a capping inversion. They describe negative vertical wind speeds 10 km downstream of a wind farm at both wake edges, which are not completely symmetrical. These downdrafts could hint at circulation zones at both wake edges which could be related to secondary flow of the second kind. The presence of Coriolis force and small veer could have caused the asymmetries. Similarly, this could mean that the circulation described in our results is partly influenced by Prandtl secondary flow, in addition to further processes that could be relevant in a CNBL.

Our results showed that the northern circulation zone can cause a speed-up at hub height altitudes (Fig. 15(6)), which spans over multiple kilometres in crosswise and streamwise direction, and could increase the power production of turbines in these areas. A speed-up at one side of the wake was already described by Nygaard and Hansen (2016). They derived wind speeds from wind turbine data of the Nysted and Rodsand II wind farms, before and after construction of the latter wind farm. For westerly wind direction the Nysted wind farm is mostly in the wake of the Rodsand II wind farm and thus shows mostly decreased wind speeds after the construction of Rodsand II. However, turbines next to the northern wake edge had increased wind speeds by almost 0.5 $\mathrm{ms^{-1}}$ compared to before the construction, indicating a speed-up region created by the upstream wind farm, which had a similar order of magnitude as our baseline setup. It is however not possible to say whether the speed-up region was similar to our results only present at one wake edge, or whether a similar speed-up region also existed at the other wake edge, since no turbines and thus no measurements were located there.

4.4 Influence on the wake of a downstream wind farm and power production

Previous studies described vertical staggering as a potential way to increase the power production of a wind farm (Sun and Yang, 2023; Vasel-Be-Hagh and Archer, 2017), which is confirmed by our results and related to higher wind speeds at higher

https://doi.org/10.5194/wes-2026-140
Preprint. Discussion started: 10 September 2026

eawe european academy of wind energy
Open Access WIND ENERGY SCIENCE DISCUSSIONS

altitudes, a lower turbine density per height, and the internal wind farm wake recovery.

Our results align with previous studies describing that wakes of upstream wind farms can still persist inside and around downstream wind farms (Schneemann et al., 2020; Stieren and Stevens, 2022). The main effect is thereby visible in the first few rows (Nygaard and Hansen, 2016). In our results this became visible as wake heterogeneities persist inside and downstream of a second wind farm and remains of the circulation zones of S1 still exist in the first few rows of the downstream wind farm. The power can still be affected throughout the entire wind farm, as indicated by our vertical staggering results as well as Stieren and Stevens (2022).

Locally, the power production of a downstream wind farm can be affected by heterogeneities in the flow caused by the wake of an upstream wind farm. For example, the speed-up region at the northern wake boundary increases the power production of the first few turbines in the northern column. Similarly, Nygaard and Hansen (2016) described for certain wind directions higher wind speeds that are related to a larger power production of turbines at the left side of the wind farm. Stieren and Stevens (2022) found a larger power production at the northern column due to entrainment of less disturbed flow from above. Vertical entrainment of higher wind speeds result for our column setup (S1) also in locally increased power production inside the downstream wind farm. For our setup S1 the wake heterogeneities thus result in an overall increased power despite the stronger mean wake.

Behind the downstream wind farm Stieren and Stevens (2022) found a faster wake recovery due to increased turbulence caused by the upstream wind farm. We similarly found a faster wake recovery behind the downstream wind farm for all analysed setups, which is however mainly related to a stronger crosswise advection and partly the decreasing wake width that results in including more wake-adjacent regions with higher wind speeds to be included in the calculation of the mean wake deficit. These differences of the dominating recovery mechanism could be explained by the different atmospheric conditions, since Stieren and Stevens (2022) simulated an atmosphere with no capping inversion and barely any veer. These two factors influence first, the northern circulation zone and second, the deflection around the wind farm. In our cases, the northern circulation zone strengthened behind the downstream wind farm more than behind the upstream wind farm, causing the strong crosswise advection. This strong circulation zone is likely not present for Stieren and Stevens (2022). A capping inversion can further cause a stronger crosswise deflection that results in flow advection into the wake behind the wind farm, especially if the capping inversion is close to the wind farm top, such as in our vertical staggering cases.

4.5 Restrictions of the setup

Looking at the specific influences of our vertical staggering setups, we found that the presence of wake heterogeneities can strongly affect the power production of a downstream wind farm. We suspect that the location of the heterogeneities and circulation zones with respect to the downstream wind turbine locations can influence whether this downstream wind farm is positively or negatively affected. Since the flow heterogeneities change in streamwise direction, the distance between the wind farms could thus also affect the overall power output. For our column staggering setup, it is therefore difficult to generalise whether an upstream staggered wind farm increases the power production of a downstream wind farm.

Further limitations of our results mainly relate to the atmospheric conditions. Changing wind directions are expected to influence the results, especially of our column staggering setups, since a deviation from the westerly direction could weaken the circulation cells inside the wind farm. If a wind farm is located at a site with a dominating wind direction, larger wind direction changes might be less relevant than smaller wind direction changes of a few degrees. The sensitivity to smaller and larger wind direction should therefore be further investigated. Similarly, the northern circulation cell could be sensitive to the wind direction, since a long wind farm and sharp wake edge might be required for its formation and strengthening. As Nygaard and Hansen (2016) described, a speed-up only exists for a small wind direction range. Since these circulation cells also showed to be affected by the capping inversion (Lanzilao and Meyers, 2025), it would further be interesting to investigate how the vertical staggering results are influenced, or to generalise, how the wind farm height with respect to the boundary layer height affects the formation and strength of the northern circulation zone.

5 Conclusions

With our LES study we aim to understand how the wind farm wake and wake recovery mechanisms in a conventionally neutral boundary layer are affected by vertically staggered wind farms and investigate whether vertical staggering could mitigate wake effects on a downstream non-staggered wind farm. We found that vertical staggering in a conventionally neutral boundary layer with wind turbines reaching up close to the capping inversion can have far-reaching influences on the wake extent, intensity, heterogeneity, and recovery, which impacts the wake development and power production of a downstream wind farm. Vertical staggering increases the power production of the upstream wind farm due to wind shear effects and an increased turbine spacing at the two height levels of the wind farm and the corresponding improved internal wake recovery. Related to that, wind speeds at higher altitudes decrease and hinder wake recovery at the hub height of the lower turbines. Consequently, the mean cluster wake recovery of vertically staggered wind farms is mostly negatively affected and causes a smaller power production of a non-staggered downstream wind farm for most vertical staggering cases. However, streaks with increased wind speeds can form behind vertically staggered wind farms, resulting in locally higher power production in the downstream wind farm.

The wake recovery mechanisms of vertically staggered wind farms are dominated by advective momentum transport throughout the streamwise extent of the farm wake, which is partly related to circulation zones in the flow. The forming mechanisms of these circulation zones are not clear yet and need further investigation. Especially interesting is the formation of a circulation zone at the side of the wake the Coriolis force is acting from, so on the northern hemisphere the left wake side, seen from above in streamwise direction. This circulation zone exists also for the non-staggered setup, but is stronger for the vertically staggered wind farms and results in a speed-up region and crosswise entrainment into the wake, which results especially in

https://doi.org/10.5194/wes-2026-140
Preprint. Discussion started: 10 September 2026

the far cluster wake in a stronger wake recovery and a smaller wake width. Vertically staggered and non-staggered wind farms can have far reaching effects on a second downstream wind farm, with an increased wake recovery rate caused by stronger crosswise entrainment. The strength of this effect differs depending on the setup and is stronger for the vertical staggering cases due to a stronger circulation zone at the left wake boundary. Some of our results might be related to the specific atmospheric conditions and wind farm setup, requiring further investigations to analyse their sensitivity and allow generalisations.

Overall, we provide first results on the impacts of vertically staggered wind farms on the flow and power production. We give insights into wake recovery processes beyond vertically staggered wind farms and show the importance of analysing the three-dimensional flow field in realistic boundary layers. Our gained understanding on factors that influence advective wake recovery processes could be used in future to investigate further methods that might enhance cluster wake recovery via advection.

Code and data availability. The PALM model software is open source and available at https://docs.palm-model.com/25.04/. The namelist input file of the precursor and baseline run is available at https://doi.org/10.57782/BLNHX9. Other namelist files and the model data can be made available on request.

https://doi.org/10.5194/wes-2026-140
Preprint. Discussion started: 10 September 2026

eawe european academy of wind energy
Open Access WIND ENERGY SCIENCE DISCUSSIONS

Appendix A: Additional results and discussion

A1 Comparison of further setups

Two of our simulated setups (S4, S5) had increased turbine hub heights only in the front or the back, not throughout the entire wind farm. Overall, this resulted in weaker effects compared to the other vertical staggering setups. The differences will be described in the following.

Inside the wind farm, the wake deficit of S4 and S5 was similar as B1 regarding the magnitude and increase over the wind farm length by around $8\,\%$ (Fig. A1(a)). Still, for S5 the inner wind farm deficit at baseline hub height upstream of the last two elevated rows was stronger compared to B1 despite the identical layout in this region. This indicated an additional wind speed reduction by a blockage effect of the higher turbines. Similar conclusions can be made from the area upstream of the wind farm. Upstream of the wind farm we observed differences in the wind speed, where the mean wind speed of S3 decelerated earlier and more compared to all other setups. These differences could be related to the blockage effect, which was stronger for an overall larger height of the wind farm in the sheared boundary layer.

Behind the wind farm, S4 showed similar to B1 the typical logarithmic wake recovery in streamwise direction, which was however less strong, resulting in an overall stronger deficit of around 2 % for S4 (Fig. A1(a)). For S5 the development of the cluster wake was more similar to the other vertical staggering setups, showing a slower mean wind speed recovery in the first 30 km, partly with a slight strengthening of the deficit. These results indicate that even adding only increased turbines in the last two rows can hinder the wake recovery considerably by creating a strong wake deficit aloft (Fig. A1(c)).

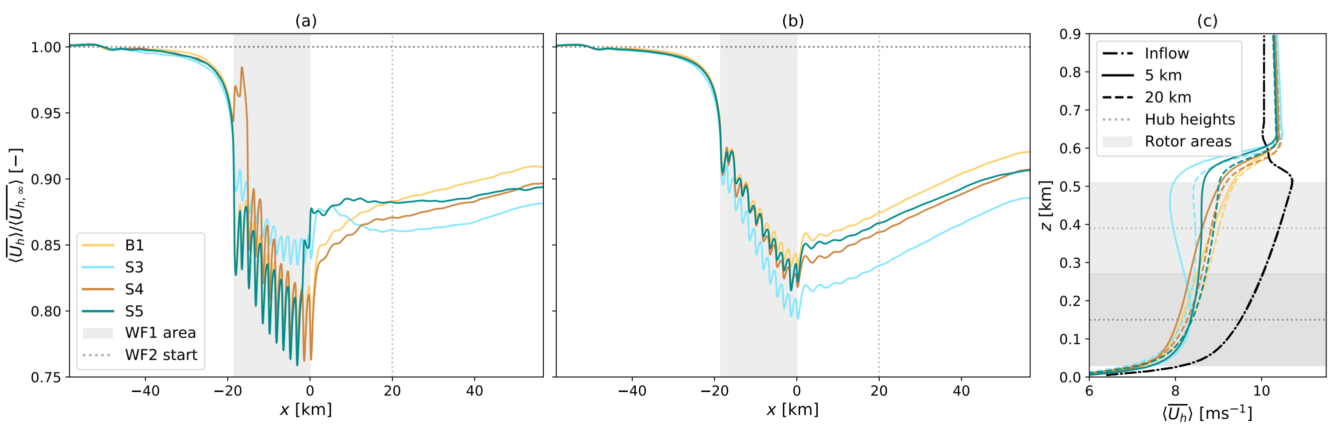

Figure A1. Horizontal wind speed averaged over the full wind farm (WF) width. (a) At the baseline hub height 150 m normalised against the inflow and plotted along the streamwise direction, where x is the distance behind the wind farm. (b) Same as (a), but instead of the baseline hub height averaged over the height of the tallest wind farm (30 m to 510 m). (c) As a vertical profile for two locations, 5 km behind the wind farm and 20 km behind the wind farm (start of potential second wind farm (WF2)).

https://doi.org/10.5194/wes-2026-140
Preprint. Discussion started: 10 September 2026

A2 Turbulent kinetic energy inside and downstream of WF1

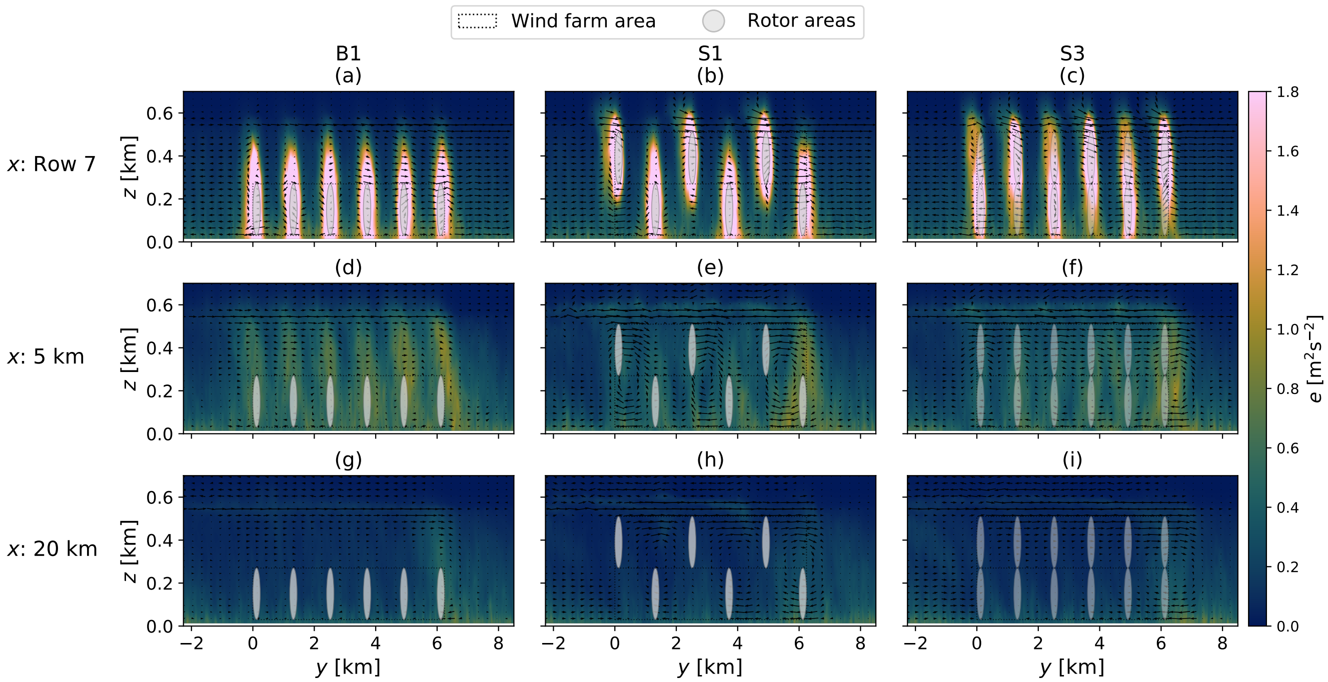

Figure A2. Vertical slices of the TKE (colormap) and the flow field displayed as arrows ($v - v_\infty$ and $w - w_\infty$). The slices are (a,b,c) between the seventh and eighth turbine row, (d,e,f) 5 km downstream of the wind farm, and (g,h,i) 20 km downstream of the wind farm. The plots are shows for (a,d,g) B1, (b,e,h) S1, and (c,f,i) S3.

800 *Author contributions.* AG set-up and performed the simulations, carried out the analysis, and wrote and edited the manuscript. GS, GC and MK reviewed the manuscript, provided new ideas and contributed to the discussion of the setup and results. GS and GC contributed to of the acquisition of the project C^2-Wakes under which the research was carried out. GS, AG and GC acquired the granted computing time at the supercomputer Emmy/Grete at NHR-Nord@Göttingen, where the simulations were carried out.

Competing interests. The authors declare that they have no conflicts of interest.

https://doi.org/10.5194/wes-2026-140
Preprint. Discussion started: 10 September 2026

Acknowledgements. This work is funded by the Federal Ministry for Economic Affairs and Energy according to a resolution by the German Federal Parliament (project C^2-Wakes, grant no. 03EE3087B). The authors gratefully acknowledge the computing time granted by the Resource Allocation Board and provided on the supercomputer Emmy/Grete at NHR-Nord@Göttingen as part of the NHR infrastructure. The calculations for this research were conducted with computing resources under the project nik00084. Additional test simulations were conducted on the HPC cluster MOUSE funded by the Federal Ministry for Economic Affairs and Energy (BMWE) under grant number 03EE3067A.

References

Anderson, W., Barros, J. M., Christensen, K. T., and Awasthi, A.: Numerical and experimental study of mechanisms responsible for turbulent secondary flows in boundary layer flows over spanwise heterogeneous roughness, Journal of Fluid Mechanics, 768, 316–347, https://doi.org/10.1017/JFM.2015.91, 2015.

Borgers, R., Meyers, J., and van Lipzig, N. P.: Energy production and inter-farm wake losses in future North Sea wind farms, Environmental Research Letters, 20, 074 036, https://doi.org/10.1088/1748-9326/ADD8A2, 2025.

Boudreau, M. and Dumas, G.: Comparison of the wake recovery of the axial-flow and cross-flow turbine concepts, Journal of Wind Engineering and Industrial Aerodynamics, 165, 137–152, https://doi.org/10.1016/J.JWEIA.2017.03.010, 2017.

Centurelli, G., Peinke, J., Djath, B., Schulz-Stellenfleth, J., and Steinfeld, G.: Asymmetric behaviour of turbulence in the wake of wind farms caused by the Coriolis force, https://arxiv.org/abs/2510.26398, 2025.

Chamorro, L. P., Tobin, N., Arndt, R. E., and Sotiropoulos, F.: Variable-sized wind turbines are a possibility for wind farm optimization, Wind Energy, 17, 1483–1494, https://doi.org/10.1002/WE.1646, 2014.

Chatterjee, T. and Peet, Y.: Exploring the benefits of vertically staggered wind farms: Understanding the power generation mechanisms of turbines operating at different scales, Wind Energy, 22, 283–301, https://doi.org/10.1002/WE.2284, 2019.

Crameri, F., Shephard, G. E., and Heron, P. J.: The misuse of colour in science communication, Nature Communications, 11, 1–10, https://doi.org/10.1038/s41467-020-19160-7, 2020.

Foloppe, B., Dewitte, L., and Munters, W.: Exploring cooperation between wind farms: a wake steering optimization study of the Belgian offshore wind farm cluster, Journal of Physics: Conference Series, 2505, 12 055, https://doi.org/10.1088/1742-6596/2505/1/012055, 2023.

Gaertner, E., Rinker, J., Sethuraman, L., Zahle, F., Anderson, B., Barter, G., Abbas, N., Meng, F., Bortolotti, P., Skrzypinski, W., Scott, G., Feil, R., Bredmose, H., Dykes, K., Shields, M., Allen, C., and Viselli, A.: Definition of the IEA Wind 15-Megawatt Offshore Reference Wind Turbine, Tech. rep., Golden, CO: National Renewable Energy Laboratory (NREL), https://www.nrel.gov/docs/fy20osti/75698.pdf, NREL/TP-5000-75698., 2020.

Gutknecht, J., Becker, M., Taschner, E., Stipa, S., Allaerts, D., Viré, A., and Wingerden, J.-W. V.: Active Cluster Wake Mixing, Journal of Physics: Conference Series, 2767, 092 052, https://doi.org/10.1088/1742-6596/2767/9/092052, 2024.

Kasper, J. H. and Stevens, R. J.: Effects of wind turbine rotor tilt on large-scale wind farms, Journal of Physics: Conference Series, 2767, 092 072, https://doi.org/10.1088/1742-6596/2767/9/092072, 2024.

Kasper, J. H. and Stevens, R. J. A. M.: From turbine-scale to wind farm-scale wake recovery: Understanding the transition, Journal of Renewable and Sustainable Energy, 18, 13 302, https://doi.org/10.1063/5.0285347, 2026.

Laan, M. P. V. D. and Sørensen, N. N.: Why the Coriolis force turns a wind farm wake clockwise in the Northern Hemisphere, Wind Energ. Sci, 2, 285–294, https://doi.org/10.5194/wes-2-285-2017, 2017.

Lanzilao, L. and Meyers, J.: Wind-farm wake recovery mechanisms in conventionally neutral boundary layers, Journal of Fluid Mechanics, 1015, A5, https://doi.org/10.1017/JFM.2025.10320, 2025.

Li, Y., Yu, W., Sciacchitano, A., and Ferreira, C.: Numerical investigation of regenerative wind farms featuring enhanced vertical energy entrainment, Wind Energy Science, 10, 631–659, https://doi.org/10.5194/wes-10-631-2025, 2025.

Lu, P., Wang, Y., Zhou, Y., Ge, M., and Li, R.: Large-eddy simulation of wind farm wake behavior and power efficiency: Effects of atmospheric stratification and staggered configurations, Renewable Energy, 249, 123 075, https://doi.org/10.1016/j.renene.2025.123075, 2025.

https://doi.org/10.5194/wes-2026-140
Preprint. Discussion started: 10 September 2026

WIND ENERGY SCIENCE DISCUSSIONS

Maas, O. and Raasch, S.: Wake properties and power output of very large wind farms for different meteorological conditions and turbine spacings: a large-eddy simulation case study for the German Bight, Wind Energy Science, 7, 715–739, https://doi.org/10.5194/wes-7-715-2022, 2022.

Maronga, B., Banzhaf, S., Burmeister, C., Esch, T., Forkel, R., Fröhlich, D., Fuka, V., Gehrke, K. F., Geletič, J., Giersch, S., Gronemeier, T., Groß, G., Heldens, W., Hellsten, A., Hoffmann, F., Inagaki, A., Kadasch, E., Kanani-Sühring, F., Ketelsen, K., Khan, B. A., Knigge, C., Knoop, H., Krč, P., Kurppa, M., Maamari, H., Matzarakis, A., Mauder, M., Pallasch, M., Pavlik, D., Pfafferott, J., Resler, J., Rissmann, S., Russo, E., Salim, M., Schrempf, M., Schwenkel, J., Seckmeyer, G., Schubert, S., Sühring, M., Tils, R. V., Vollmer, L., Ward, S., Witha, B., Wurps, H., Zeidler, J., and Raasch, S.: Overview of the PALM model system 6.0, Geoscientific Model Development, 13, 1335–1372, https://doi.org/10.5194/GMD-13-1335-2020, 2020.

Nygaard, N. G. and Hansen, S. D.: Wake effects between two neighbouring wind farms, Journal of Physics: Conference Series, 753, 032 020, https://doi.org/10.1088/1742-6596/753/3/032020, 2016.

Ouro, P., Ghobrial, M., Ali, K., and Stallard, T.: Numerical modelling of offshore wind-farm cluster wakes, Renewable and Sustainable Energy Reviews, 215, 115 526, https://doi.org/10.1016/J.RSER.2025.115526, 2025.

Paulsen, J., Steinfeld, G., Kühn, M., and Dörenkämper, M.: Mitigation of offshore wind farm cluster wake effects by low-specific-rating, low-induction turbines, Wind Energy Science Discussions [preprint], https://doi.org/10.5194/wes-2026-23, in review, 2026.

Platis, A., Siedersleben, S. K., Bange, J., Lampert, A., Bärfuss, K., Hankers, R., Cañadillas, B., Foreman, R., Schulz-Stellenfleth, J., Djath, B., Neumann, T., and Emeis, S.: First in situ evidence of wakes in the far field behind offshore wind farms, Scientific Reports, 8, 1–10, https://doi.org/10.1038/s41598-018-20389-y, 2018.

Schneemann, J., Rott, A., Dörenkämper, M., Steinfeld, G., and Kühn, M.: Cluster wakes impact on a far-distant offshore wind farm's power, Wind Energy Science, 5, 29–49, https://doi.org/10.5194/WES-5-29-2020, 2020.

Stieren, A. and Stevens, R. J. A. M.: Impact of wind farm wakes on flow structures in and around downstream wind farms, Flow, 2, 21, https://doi.org/10.1017/flo.2022.15, 2022.

Sullivan, P. P., Moeng, C.-H., Stevens, B., Lenschow, D. H., and Mayor, S. D.: Structure of the Entrainment Zone Capping the Convective Atmospheric Boundary Layer, Journal of the Atmospheric Sciences, 55, 3042–3064, https://doi.org/10.1175/1520-0469(1998)055<3042:SOTEZC>2.0.CO;2, 1998.

Sun, H. and Yang, H.: Wind farm layout and hub height optimization with a novel wake model, Applied Energy, 348, 121 554, https://doi.org/10.1016/j.apenergy.2023.121554, 2023.

Syed, A. H., Javed, A., Feroz, R. M. A., and Calhoun, R.: Partial repowering analysis of a wind farm by turbine hub height variation to mitigate neighboring wind farm wake interference using mesoscale simulations, Applied Energy, 268, 115 050, https://doi.org/10.1016/J.APENERGY.2020.115050, 2020.

Syed, A. H., Mann, J., Platis, A., and Bange, J.: Turbulence structures and entrainment length scales in large offshore wind farms, Wind Energ. Sci, 8, 125–139, https://doi.org/10.5194/wes-8-125-2023, 2023.

Vanderwel, C. and Ganapathisubramani, B.: Effects of spanwise spacing on large-scale secondary flows in rough-wall turbulent boundary layers, Journal of Fluid Mechanics, 774, R2, https://doi.org/10.1017/JFM.2015.292, 2015.

Vasel-Be-Hagh, A. and Archer, C. L.: Wind farm hub height optimization, Applied Energy, 195, 905–921, https://doi.org/10.1016/j.apenergy.2017.03.089, 2017.

Wang, Y., Lu, P., Zhou, Y., Guan, R., and Li, R.: Insight into the impact of turbine-array configurations on the power output and wake effects of a finite-size wind farm, Renewable Energy, 255, 123 745, https://doi.org/10.1016/j.renene.2025.123745, 2025.

https://doi.org/10.5194/wes-2026-140
Preprint. Discussion started: 10 September 2026

Wu, Y.-T., Porté-Agel, F., t Wu, Y., and Porté-Agel, F.: Large-Eddy Simulation of Wind-Turbine Wakes: Evaluation of Turbine Parametrisations, Boundary-Layer Meteorology, 138, 345–366, https://doi.org/10.1007/s10546-010-9569-x, 2011.

Wu, Y.-T., Liao, T.-L., Chen, C.-K., Lin, C.-Y., and Chen, P.-W.: Power output efficiency in large wind farms with different hub heights and configurations, Renewable Energy, 132, 941–949, https://doi.org/10.1016/j.renene.2018.08.051, 2018.

Zhang, M., Arendshorst, M. G., and Stevens, R. J.: Large eddy simulations of the effect of vertical staggering in large wind farms, Wind Energy, 22, 189–204, https://doi.org/10.1002/WE.2278, 2018.